ADDIS ABABA UNIVERSITY

ADDIS ABABA INSTITUTE OF TECHNOLOGY

SCHOOL OF MECHANICAL AND INDUSTRIAL ENGINEERING

EFFECT OF CHANGE OF WHEEL-RAIL CONTACT GEOMETRY ON CONTACT FATIGUE STRESSES

A master's thesis submitted to the school of mechanical and industrial of Addis Ababa University in partial fulfillment of the requirements for the degree of Master of Science in mechanical engineering under railway program.

By

Fikru Bekele

Advisors

Dr.Daniel Tilahun,

Habtamu Tikubet.

August, 2014

Acknowledgment

First of all I would like to express my sincere appreciation and gratitude to Dr. Daniel Tilahun and Habtamu Tikubet for being my advisors and for their invaluable support and guidance in every steps of this thesis. Without their guidance and support this work would have been impossible.

I am also very grateful to Behailu Tasew (staff in mechanical engineering department) for his invaluable CATIA training.

Special thanks goes to Dr Daniel Tilahun for his interesting course Research Methodology for he has inspired me to conduct research and for enlightening me about the basics of research methodology.

I am also very grateful to all my colleagues at department of mechanical engineering for your fruitful discussions. My special thanks go to you for all we have been through

To my family whose support and encouragement made this work possible, you deserve my deepest gratitude and love. Thank you.

Abstract

The general objective of this thesis is to analyze effect of change of wheel and rail profiles on contact fatigue stress using analytic and finite element softwares. The wheel rail contact condition is modeled assuming two general quadratic surfaces. The formulation in this study aims primarily at determination of stresses and fatigue parameters by varying contact geometry arising from variation in profile geometry. A change in surface geometry brings in a change in contact geometry and stresses. The theoretical models are based on the normal problem (Hertz theory) and the tangential problem (Kalker's theory). Correspondingly, variations in the results in terms of principal stresses and fatigue parameters such as equivalent stresses, fatigue damage, and expected fatigue life with changes in wheel profile radii, wheel taper and rail profile radii are obtained. Comparisons of different profiles are taken place. Better profiles are suggested. Results obtained are expected to help understand the rail wheel configuration dependence on the stress deformation pattern and fatigue parameters. This may help an appropriate selection of wheel and rail profiles in the optimization process.

Table of Contents

List of Figures

List of tables

List of symbols

FI_{surf}	Surface fatigue index
μ	Traction coefficient
$\boldsymbol{a}$	Major axes of the hertizian contact patch
$\boldsymbol{b}$	Minor axes of the hertizian contact patch
$\boldsymbol{\delta}$	Deformation
F_z	The normal force magnitude
F_x	Longitudinal creep force
F_y	Lateral creep force
z	Surface shape function of body
A_1	Longitudinal curvature of curvature of body 1
A_2	longitudinal curvature of curvature of body 2
B_1	Transversal curvature of curvature of body 1
B_2	Transversal curvature of curvature of body 2
$\boldsymbol{\gamma}$	Conicity
r_n	The normal radius of the wheel
r_o	The rolling radius of the wheel
$\boldsymbol{R_{wx}}$	Radius of curvature of the wheel
$\boldsymbol{R_{rx}}$	Radius of curvature of the rail
E	Young’s modulus of elasticity

v	The Poisson's ratio
m	Nondimensional coefficients tabulated as a function of the ratio g = n/m or the angle Θ
n	Nondimensional coefficients tabulated as a function of the ratio g = n/m or the angle Θ
r	Nondimensional coefficients tabulated as a function of the ratio g = n/m or the angle Θ
N	The vertical load applied normal to the contact patch
σ_{max}	The maximum pressure will be simply
V_T	Translational velocity
V_C	Circumferential velocity
ξ	Longitudinal creepage
η	Lateral creepage
φ	Rotational creepage
Ω_x	Rotation of the wheel around x-axes
Ω_y	Rotation of the wheel around y-axes
Ω_z	Rotation of the wheel around z-axes
α	The yaw angle
γ	Conicity
y	Lateral displacement of the wheelset
r_o	Rolling radius of the wheel.
L	Elasticity coefficient
p_m	The mean contact stress
p_o	The maximum contact stress

$\boldsymbol{p(x, y)}$ The pressure distribution within the contact ellipse

$\boldsymbol{\sigma_x}$ The principal direct stresses acting along the x axes at or below, the contact center

$\boldsymbol{\sigma_y}$ The principal direct stresses acting along the y axes at or below, the contact center

$\boldsymbol{\sigma_z}$ The principal direct stresses acting along the z axes at or below, the contact center

$\boldsymbol{\tau}_1$ The maximum principal shear stress in the plane of deformation

K The yield stress in simple shear

$\boldsymbol{Y}$ The yield stress in simple tension

$\boldsymbol{\sigma_h}$ The hydrostatic stress

$\boldsymbol{\tau}_{\max}$ The maximum principal shear stress

$\boldsymbol{\tau_a}$ The shear stress amplitude

$\boldsymbol{\tau_e}$ The fatigue limit in alternating shear

$\boldsymbol{\sigma_e}$ The fatigue limit in rotating bending

$\boldsymbol{a_{DV}}$ The Dang Van material parameter

$\boldsymbol{\sigma_u}$ The tensile fracture stress of the material

$\boldsymbol{\sigma_{EQ}}$ Equivalent stress

$\boldsymbol{f}$ The traction coefficient

FP Fatigue parameter

$\Delta\boldsymbol{\varepsilon}$ The range of the normal strain

$\Delta\,\boldsymbol{\vartheta}$ The range of the (engineering) shear strain

$\Delta\boldsymbol{\tau}$ The range of the shear stress

E	Young's elasticity modulus
σ_f'	Additional material parameter
ε_f'	Additional material parameter
b	Additional material parameter
c	Additional material parameter
ε_i	The current strain increment
ε_c	The fracture strain
$q(x,y)$	The shear stress traction in the wheel-rail interface
D	Fatigue damage per cycle
S_u	Ultimate (equivalent) strength
σ_e	Equivalent fatigue limit (endurance limit)
N_f	Expected fatigue life.
W	Wear index

Chapter One

1.1 Introduction

Wheel-rail analysis has focused mainly on what is known as rolling contact fatigue. This phenomenon arises primarily where there are contacts with low relative sliding, such as on the rail head on straight tracks. [Tanel Telliskivi, 2003]

Wheel/rail contact physically occupies an area the size of a small coin. And such contact transfers the load from a vehicle ranging from 3.5 t (28 t lightweight passenger coach) to 17.5 t (heavy freight car of 140 t) per wheel. The material in and around the contact area is therefore highly stressed. High rates of wear might be expected from such contact and, because the load is applied and removed many times during the passage of each train, there is the added possibility of fatigue of the rail surface. [Ivan Y. Shevtsov, 2008]

The nature of the fit between contacting bodies is divided into two types namely conformal and nonconformal. Conformal contact occurs where the surfaces contact uniformly over their contacting boundaries resulting in a large contact area in relation to the size of the contacting objects. This contact generates a stress field which propagates uniformly throughout the bodies and is tied to the general stress field of the bulk of the bodies. Non-conformal contact on the other hand begins in the form of point or line contact which develops with increasing loading into a contact patch with a small contact area in relation to the size of the contacting bodies. In general cases this patch is of an elliptical shape and depends on the orthogonal radii of curvature at the contact point of the contacting bodies. This results in local stress concentrations and stresses in the region of contact much greater than the general stresses in the bulk of the bodies. The case of railway wheel/rail interaction falls into the non conformal category with two possible contact regions being present. The wheel-tread/rail-head contact is always present and results in the development of a contact patch those changes in shape with the loading conditions and the transverse location of the wheel on the rail. It is the dominant contact for drive traction, braking and self-steering. The wheel-flange/rail-head contact is not always present and forms the hard limit for the motion of the wheel for linear movement transverse to the rail as well as for angular misalignment of the axle. This patch has the dominant role in extreme hunting phenomenon and train steering. [Paul Boyd, 2002]

In railway infrastructure in order to increase the speed of trains, to increase the axles loads of trains and locomotives traction, to increase the density of traffic and to increase resistance to harmful influences of the environment (environmental aspects), requires improved quality of rails. Rails as an important part of the railway infrastructure have exact level of quality. In Europe, the quality of rails is prescribed by international standards, the European Union of Railways UIC 860 and EN13674. [Branislav Sladojevic, 2010]

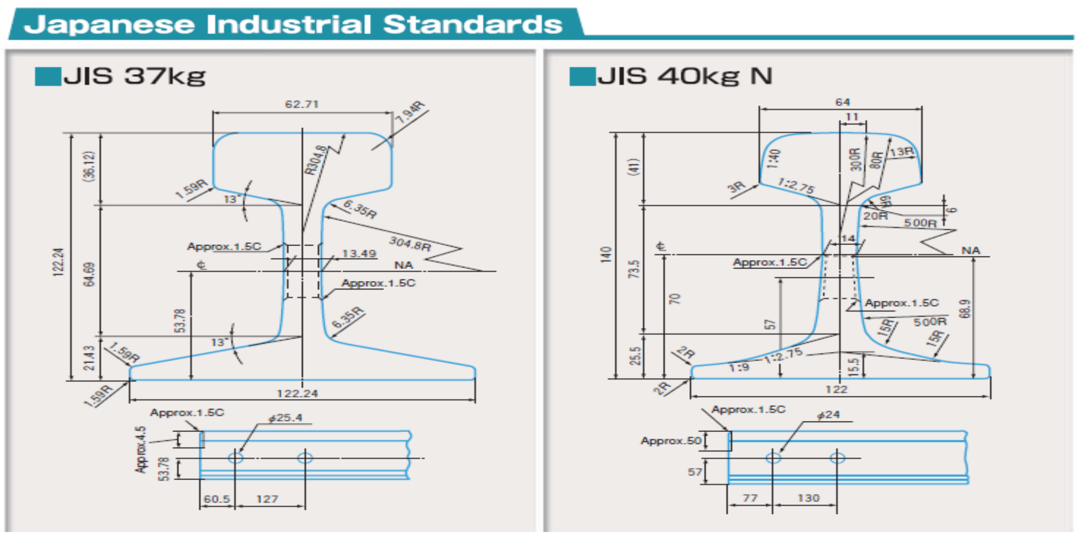

Figure 1.1: Typical japanese standard rails

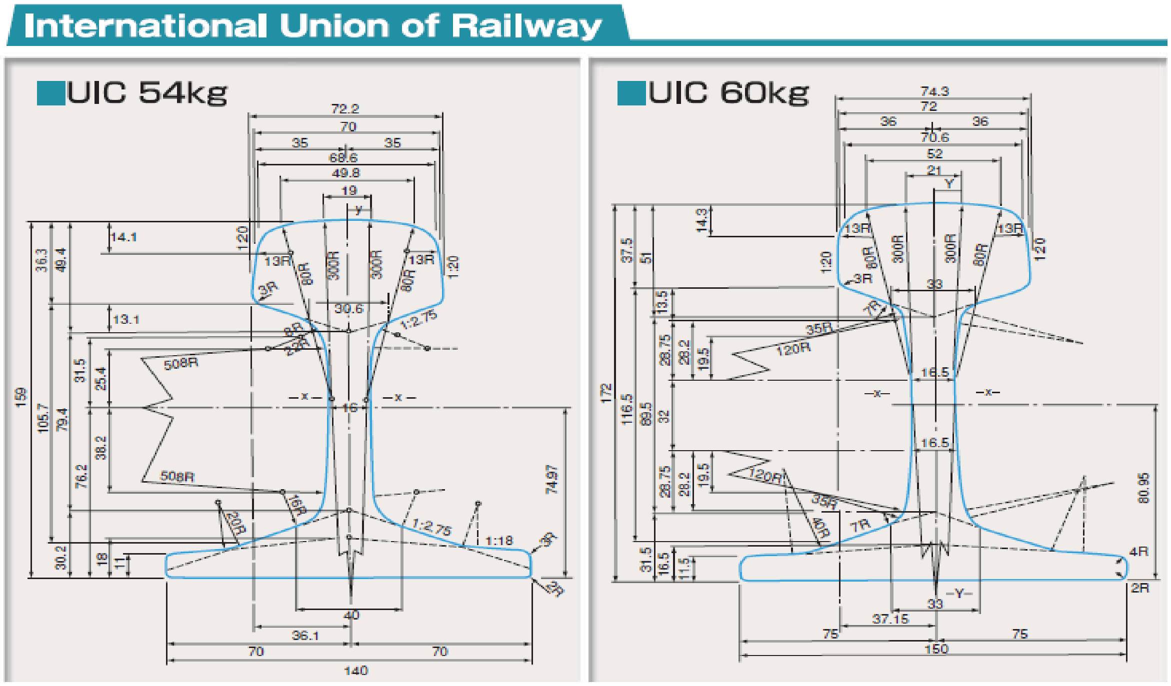

Figure 1.2:Typical UIC standard rails

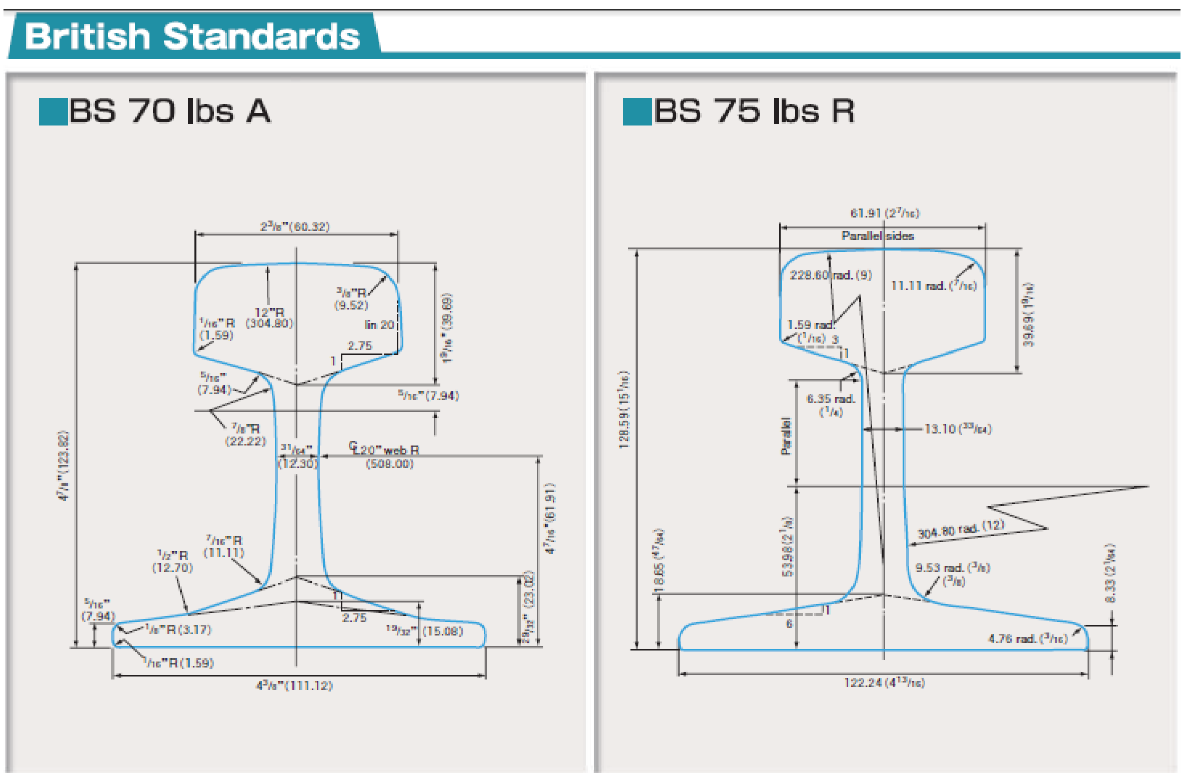

Figure 1.3:Typical British standard rails

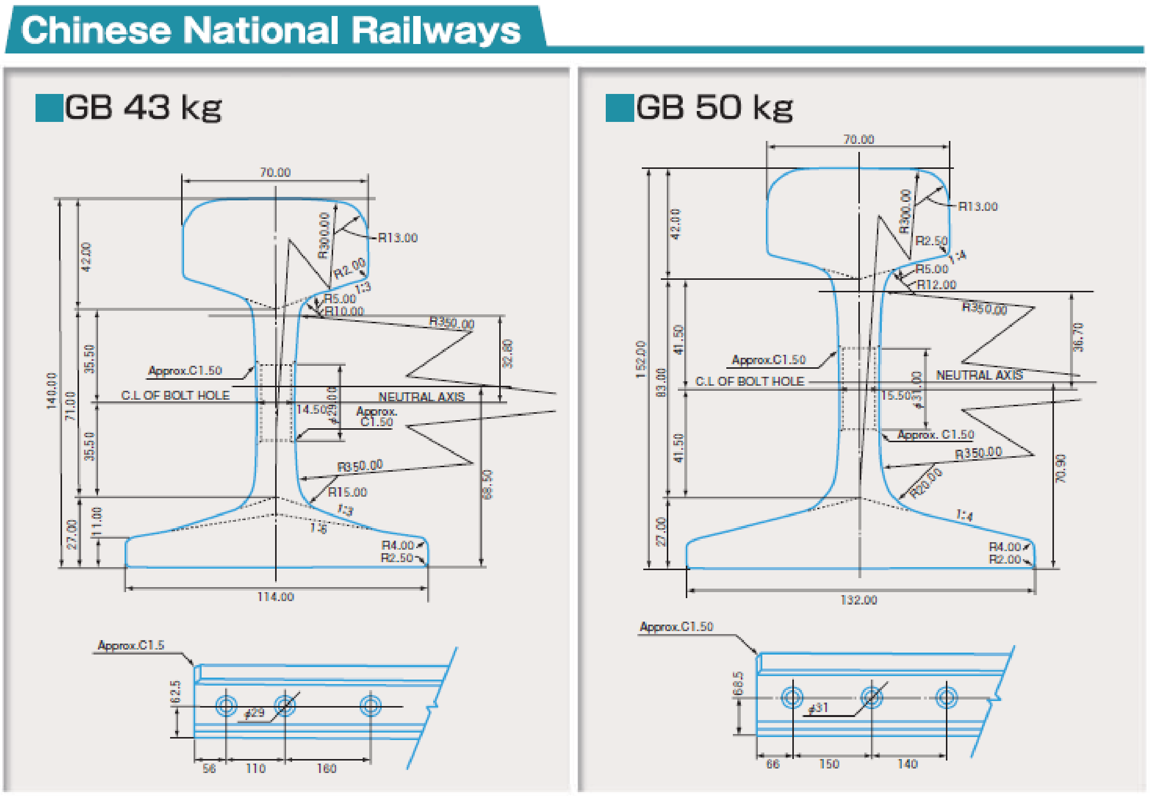

Figure 1.4:Typical chinese standard rails

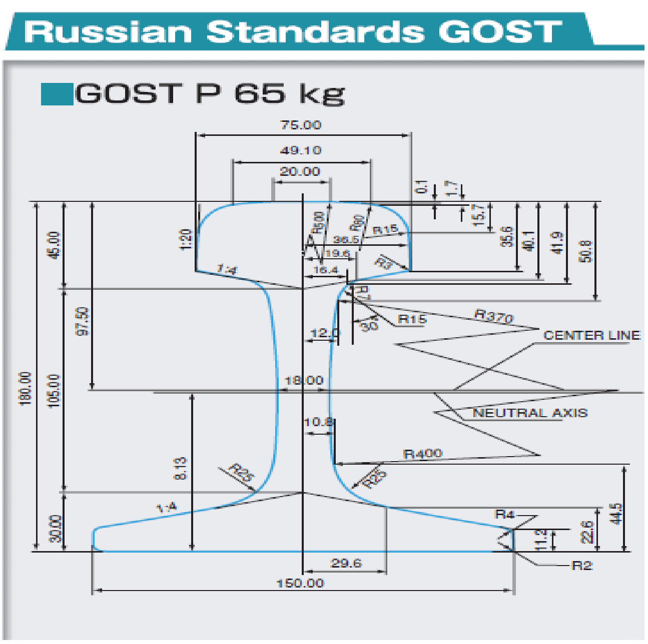

Figure 1.5:Typical russian standard rails

1.2 Rolling contact fatigue problem:

The prediction of surface fatigue defects (head checks) is defined by the surface fatigue index FI_{surf} :

$$FI_{surf} = \mu - \frac{2\pi abk}{3\ F_z} > 0 \qquad 1.1$$

Where μ is the traction coefficient, *a*, *b* are the semiaxes of the Hertzian contact patch, F_z is the normal force magnitude, and *k* is the yield stress in pure shear. The traction coefficient μ is defined as the quotient between the tangential and normal forces in the contact patch:

$$\mu = \frac{\sqrt{F_x^2 + F_y^2}}{F_z} \qquad 1.2$$

Where F x and F y are the longitudinal and lateral creep forces.
Here we can see that the surface fatigue index is a function of the wheel rail contact patch (πab)which is determined by wheel and rail profiles combinations.

Therefore in this study an attempt is made to select a standard rail and then a compatible wheel profile will be generated. Three geometrical conditions are selected: the variation in conicity, the variation in radius of curvatures of wheel profile, and the variation in radius of curvatures of the rail profile. For each condition the rolling contact fatigue stresses condition is calculated with the help of both analytical and FE software's. Changing the three parameters of wheel and rail profiles the study will continue until a better wheel rail performance is obtained. Finally the optimal wheel and rail profile combinations to minimize rolling contact fatigue stress will be suggested.

1.3 Objective

1.3.1 General objective

The general objective of this thesis is to analyze effect of change of wheel and rail profiles on contact fatigue stress using analytic and finite element method.

1.3.2 Specific Objectives

- Modeling wheel and rail profiles using CATIA software
- Employing MATLAB and ANSYS software to carry out theoretical and finite element analysis considering different contact patches arising from various wheel and rail profile combinations and obtain the rolling contact fatigue stresses of each condition.

1.4 Research methodology

In this thesis, several theoretical and numerical approaches on wheel rail contact are employed to investigate the relationship between geometrical configurations of wheel and rail profiles with fatigue parameters. These are:

- Hertizian theory of contact for the normal problem (i.e. determinations of elliptical contact patch and contact stresses).
- Kalker's simplified theory of contact for the formulation of the tangential problem (i.e. creepage and creep forces) .
- The Dang Van criterion based on the wholer (S-N) curve is employed in order to quantify the fatigue impact.
- Finite element softwares MATLAB 7.1 and ANSYS 12.0 are employed for numerical results
- For modeling of wheel and rail CATIA V5 R16 is used

1.5 Outline

This thesis is organized in to six chapters. The first chapter illustrates the introduction, objective, and the methodology employed in this thesis work. In chapter two, a review of relevant literature to the research, which has been established by different researchers, is given. Chapter three is about contact mechanics, and how to use Hertz and Kalker's contact theory and its relations in wheel-rail contact fatigue stress analysis. In addition, all important theories and formulas necessary for the numerical calculation in the MATLAB program are established. In chapter four, finite element softwares CATIA V5 R16 and ANSYS12.0 are employed to find finite element results moreover 3D finite element analysis mechanisms and steps of ANSYS workbench are discussed. In Chapter five the results and discussion of the study are presented. The conditions of fatigue stress and fatigue life with respect to wheel and rail profile variation is discussed. Finally, chapter six discuses conclusion, recommendations and future works of this thesis work.

Chapter Two

Literature review

The study of rolling contact, or more accurately rolling-sliding contact, is said to be started in 1926 by the publication of Carter's paper [F. Carter, 1926] on the solution of the two-dimensional rolling contact problem. The three-dimensional rolling contact including sliding was touched upon by Johnson [K. Johnson, 1985] about thirty years later. His theory was approximate. Kalker continued to study the subject. He published several theories among which there is a complete theory of three-dimensional rolling contact. Using his theory, it is possible to solve the problem numerically. However, his theory is limited by the half-space assumption. Later on, others like [Wriggers, 2002] studied the problem using FEM. Using FEM, the half-space limitation is lifted and material non-linearities can be included as well. However, it raises other issues to be dealt with.

The size and shape of the contact zone where the railway wheel meets the rail can be calculated with different techniques. Traditionally, the Hertz theory of elliptical contacts has been used implying the following assumptions: the contact surfaces are smooth and can be described by second degree surfaces; the material model is linear elastic and there is no friction between the contacting surfaces; and the contacting bodies are assumed to deform as infinite half spaces. The half space assumption puts geometrical limitations on the contact, i.e., the significant dimensions of the contact area must be small compared with the relative radii of the curvature of each body. Especially in the gauge corner of the rail profile, the half plane assumption is questionable since the contact radius here can be as small as 10 mm. Due to its simple closed form solutions; the Hertz method is the most commonly used approach in vehicle dynamics simulation. However, other methods are used for simulation of wear and surface fatigue due to the overestimation of the contact stresses attributed to the nonvalidity of the half plane assumption and nonlinear material behavior. Kalker's numerical program Contact still depends on the half space assumption, but is not restricted to elliptical contact zones. The contact surfaces are meshed into rectangular elements with constant normal and tangential stresses in each rectangular element. Telliskivi and Olofsson developed a finite element model, including plastic deformation, of the wheel – rail contact using measured wheel and rail profiles as input data. And this was illustrated in [Ulf Olofsson and Roger Lewis, 2006]

According to [Paul Boyd, 2002] the entire body of knowledge relating to contact mechanics can be traced back to the initial work done by Hertz on a simplified contact model. These initial theories were based on the theories of elasticity which were well established and were further enhanced by the development of the theories of plasticity. Kalker produced the next most significant contribution to the discipline of contact mechanics with his expansion of Hertz theories and the development of computer algorithms specifically concerned with the calculation of railway rail/wheel surface tractions which are used extensively in multi body dynamics software to provide the linkage between the railway rail and wheel.

The FEM analysis is the ultimate available solution to the contact problems which violates the underlying assumptions of Kalker's variational method. It is not bound to half-space assumption and various material properties can be considered. Moreover, more detailed friction laws than the well-known Coulomb's law can be used. However, like any numerical method, there are several numerical issues to be dealt with. [Matin Shahzamanian Sichani, 2013]

According to [Shahzamanian Sichani, 2013] FEM is a numerical method to solve partial differential equations (PDEs). It eliminates the spatial derivatives and converts the PDE into a system of algebraic equations. To do so, the bodies under investigation, considered as a continuum, are discretized into elements with certain number of nodes. The solution to the PDE using FEM is exact at the nodes; while in between the nodes it is approximated by polynomials known as shape functions.

One of the fundamental issues to deal with when investigating the wheel rail contact is the rolling contact fatigue (RCF) phenomenon. It must be emphasized that (RCF) cannot be evaluated based on normal contact stress alone since the interdependence with tractions and material strength is too intimate. According to [Eric Magel, Peter Sroba,2006] Assessing wheel/rail performance with respect to contact fatigue requires consideration of all three parameters namely : *Normal stress (Po) at wheel/rail contact* which is a function of four main factors; wheel diameter, wheel load (including possible dynamic loading), the transverse rail profile and the transverse profile of the wheel. *Rail/wheel tractions (T/N)* which develops due to a small relative slip between the rail and wheel that shears the interfacial layer in the contact zone. The level of slip (also known as creep) depends on the curving and traction demands. *Rail metallurgy* in laboratory studies generally recur two conclusions. First, for a given level of hardness, pearlitic steels are more resistant to RCF than are other structures such as bainite and martensite. Second, for any given type of steel structure, resistance to RCF increases with hardness. Much work has been carried out on wheel and rail failure due to fatigue, wear and the action of wheel and rail defects. Again these effects rely on the understanding of the stress fields present and constitute another direction for the application of this research. [Ekberg et al,1995] cites the need for accurate surface, subsurface and residual stresses in his "fatigue model for general rolling contact with application to wheel/rail damage" and cites the applications of FEA programs such as ABAQUS as suitable. [Magnus et al, 1993] also describes a model for cyclic ratcheting plasticity and the development and propagation of fatigue cracks using the ABAQUS code which appears to indicate that ABAQUS may be the software of choice for this work.

Several parameters influence the stress state in rails as illustrated in[Marine Vidaud,2009]: A non-exhaustive list of these parameters might be: axle load; asymmetric loadings where the strain will also be posed asymmetric on the rail head and the rail wheel contact will get irregular and discontinuous; wheel diameter including mismatched wheel diameters; track gauge; wheel transversal profile; rail transversal profile and profile irregularities; cant excess/deficiency where wheel sets will tend to shift and to heavily offset to the inner or outer rail respectively; welds where at too soft/flexible welds a dip will be produced or, in case too hard high spots will be produced this will both leading to geometry irregularities; hunting of wheel set in tangent tracks; string lining forces on grades tie plate cut in and poor fastening; Skewed trucks.

In the contact zone between railway wheel and rail the surfaces and bulk material must be strong enough to resist the normal (vertical) forces introduced by heavy loads and the dynamic response induced by track and wheel irregularities. The tangential forces in the contact zone must be low enough to allow moving heavy loads with little resistance, at the same time the tangential loads must be high enough to provide traction, braking, and steering of the trains. [Ulf Olofsson and Roger Lewis, 2006]

The first step in wheel/rail profile evaluation procedure is the realization of a multibody model of the complete railway vehicle and track combination. This is performed to evaluate contact specific parameters, such as wheel/rail forces, relative positions, and creepages. This was discussed in detail on [Iwnicki S. ed., 2006]

An important characteristic of contact between wheel and rail is the rolling radius of the wheel at the contact point. Consequently, the difference between the rolling radius of the right and the left wheel (rolling radius difference or RRD) as a function of the lateral displacement of a wheelset is one of the main characteristics of wheel/rail contact that defines the behavior of a wheelset on a track. Modeling of the wheel rail contact both analytical and finite element simulation softwares using rolling radius difference as a function of wheel and rail profiles were shown on. [Ivan Y. Shevtsov, 2008]

In computational modeling of railway vehicle, modification of the rolling radius difference (RRD) function can change dynamic behavior of the wheelset helping to achieve the required performance. This modified RRD function virtually corresponds to a new combination of wheel/rail profiles. For a given rail profile, one may solve the inverse problem in order to find a wheel profile to match the modified RRD function. The inverse problem can be solved using an optimization method. This idea was used as a strategic concept in the creation of the procedure for wheel profile design on [Ivan Y. Shevtsov, 2008].

Modelling and simulation of the dynamic behavior of wheel-rail interface is illustrated in detail on [Iwnicki S. ed., 2006] and [Pislaru, Crinela, 2012].

For analyzing the dynamic behavior of railway vehicles running on arbitrary tracks under arbitrary maneuvers, usually the vehicle (and maybe the necessary environment) is abstracted basically as a multibody system. According to [Gunter Schupp , 2007], A multibody system consists of rigid or elastic bodies, interconnected via massless force elements and joints. Due to the relative motion of the system's bodies, force elements generate applied forces and torques. Typical examples are springs, dampers and actuators combined to primary and secondary suspensions of railway vehicles. Contrarily, joints give rise to constraint forces by constraining the relative motion of the system's bodies. The scope of applications starts with simple single axis rotational joints and ends with highly complicated and specific ones like the so–called ‘wheel–rail joints’ guiding bodies along arbitrary tracks. Usually, the user can rely on extensive libraries of connecting elements while setting up the simulation model.

Carter described a simple 2D contact surface, but he was the first to give a rather adequate expression of the force relative to the creepage in the longitudinal direction. His method of describing the stresses in the adhesive zone was used until the 1960s. Fromm made similar observations. Rocard described the linear relationship between the yaw angle and the guiding force, for rubber tires and for railway wheels, in the lateral direction. He was particularly interested in the equivalent of the bogie hunting for cars: the shimmy phenomenon.

In the 1960s, more experimental data were available; the definitive expressions were established mainly by Johnson and Kalker, who gave an expression of the creepage stiffness introducing variable coefficients depending on the b/a ratio of the contact ellipse. This expression is the most common today.

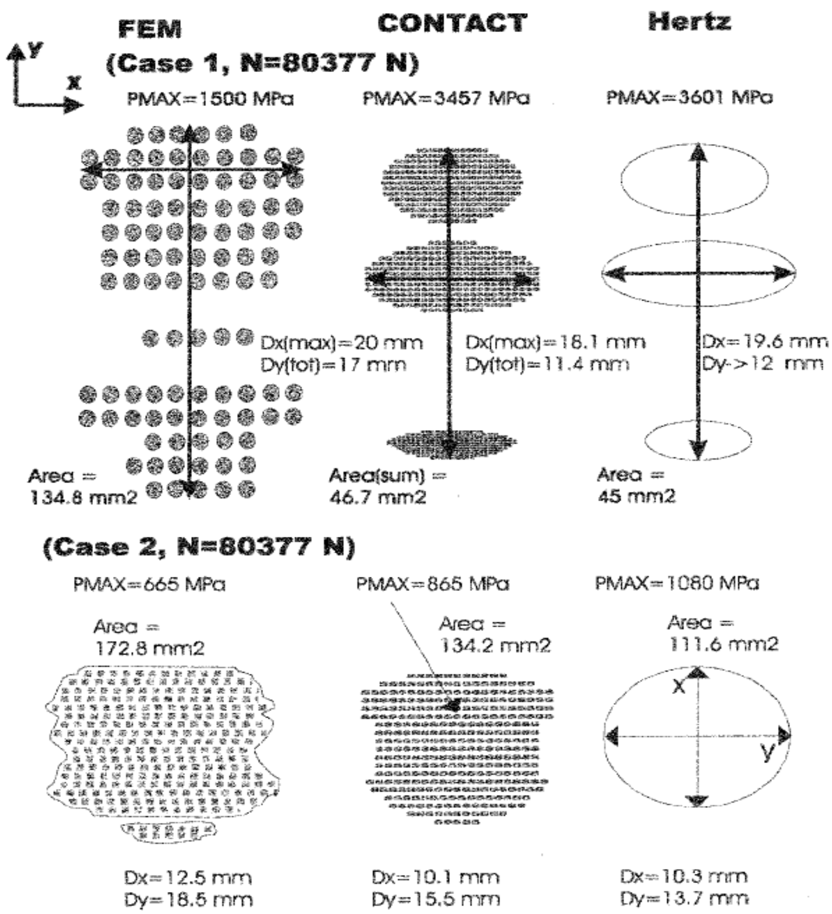

Figure 2.1: Comparison of maximum contact pressure and the contact area between three different contact methods for case 1: flange contact, and case 2: tread contact of worn profiles taken from [Matin Shahzamanian Sichani, 2013].

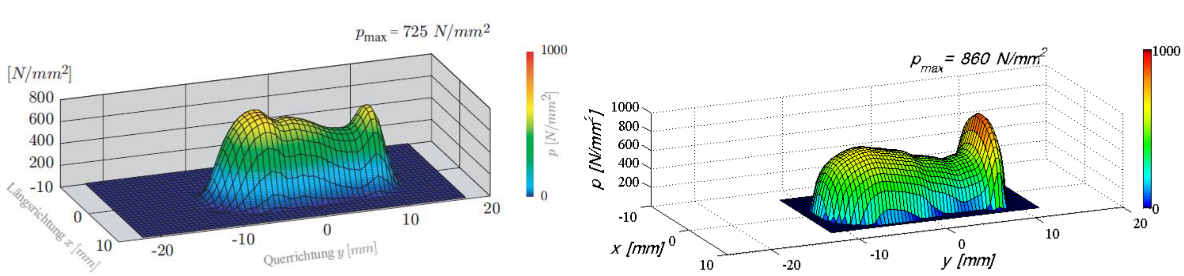

(a) (b)

Figure 2.2: Contact pressure distribution obtained by (a) FEM (from [Matin Shahzamanian Sichani, 2013], and (b) CONTACT software. Note that y-axis is positive towards gauge-corner.

Subsurface initiated rolling contact fatigue is assessed using the FIERCE model [Ekberg et al., 2002]. The fast algorithms in FIERCE allow for fatigue evaluation in each time increment. This facilitates a statistical evaluation of the fatigue impact, which is of major importance in the study of RCF of railway wheels: Since the wheels are travelling along a track with varying characteristics, they will be subjected to a broad spectrum of fatigue loading. From a fatigue point of view, mainly extreme loads are of importance since, first, fatigue initiation is related to magnitudes of fatigue impact exceeding the (equivalent) fatigue limit and, second, above the fatigue limit life is decreasing exponentially with the increase in fatigue loading.[Kabo, E., 2002]

If we look at RCF initiation deeper into the wheel rim, interfacial wheel-rail friction and the size and shape of the contact patch will have less influence. Instead, the magnitude of the total contact load and the occurrence of material defects will be the main influential factors [Kabo, 2002; Kabo and Ekberg, 2005].

[Michael Gmariam, 2013] has also studied the effect of change of contact ratios on contact fatigue stresses on spur gears. In his study he considered different cases of six contact ratios gearing between 1.6 and 2. For the different contact ratios considered different stress conditions are determined .ANSYS and CATIA finite element softwares are used for finite element results.

Chapter three

Wheel rail contact mechanics

3.1 Introduction

This chapter examines the mechanics of loaded contact between solid non-conforming bodies particularly between wheel and rail. Initially the stresses and deformations of static contact generated from a normal force are considered .The further consideration is given to the effect of relative motions between the bodies and the effect of applying tangential forces.

Even at the highest axle loads the contact area between the wheel and rail is approximately 1cm^2 i.e. the system can be viewed as a large bearing contact and, as in bearing contact, very small highly compressed regions are constrained with in a bulk of relatively unstrained material. This small area of contact with its relatively low frictional resistance means that rail vehicles are highly efficient movers of mass compared to road vehicles.

In order to Study the contact between bodies the first thing to do is to determine some contact parameters: the contact surface, the pressure and the tangential forces. This determination is generally separated into two steps:

1. The normal problem (Hertz theory)
2. The tangential problem (Kalker's theory)

The first step in the wheel – rail contact study is to consider the Hertzian modelisation starting from a simple model of the wheelset.

3.2 Hertzian Contact (normal loading of elastic, isotropic bodies without other movements)

This situation was investigated by [hertz, 1882]; his work has been described by K.L.Johnson in various papers and in his comprehensive book on contact mechanics in 1985. Some of Johnson's approach is summarized here. Two non-conforming solid bodies approaching each other must initially touch at a point except in the case of aligned cylindrical contact, where initial contact is along a line. The surface will elastically compress and form an area of contact.

Hertz demonstrates that when two elastic bodies are pressed together in the following conditions:

- Elastic behavior
- Semi-infinite spaces
- Large curvature radius compared to the contact size
- Constant curvatures inside the contact patch.
- Frictionless surface.

Then:

- The contact surface is an ellipse
- The contact surface is considered flat
- The contact pressure is a semi-ellipsoid

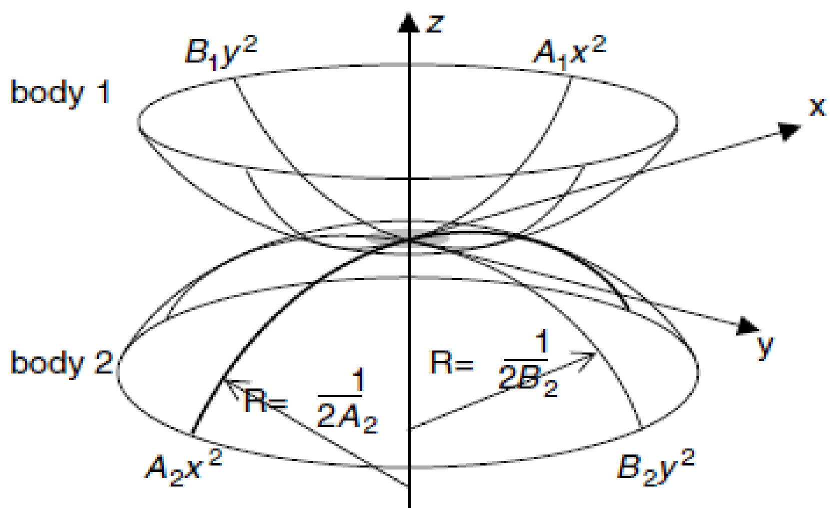

Figure 3.1: Bodies in Hertzian contact

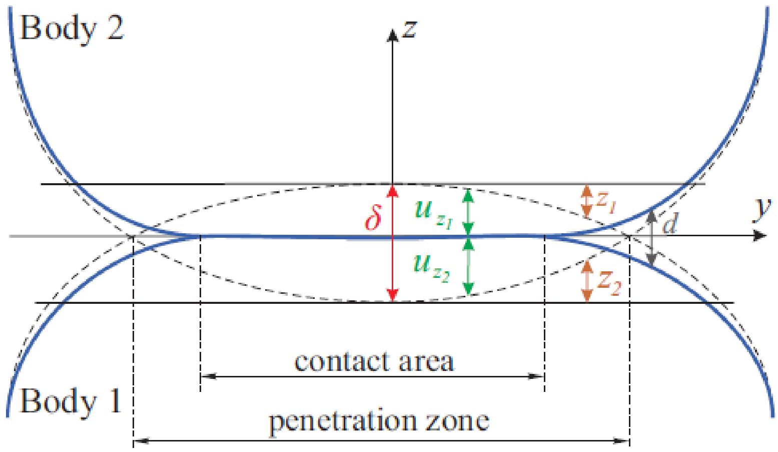

Figure 3.2: A model for elastic deformation of hertizian contact

Considering the two elastic bodies in contact, they will meet at a single point where the normal distance between them is minimal. Near this contact point, without load, the bodies' surface shapes are represented by two second order polynomials:

$$z_1 = A_1 x^2 + B_1 y^2 \qquad 3.1a$$

$$z_2 = A_2 x^2 + B_2 y^2 \qquad 3.1b$$

The $A_{1,\,2}$ and $B_{1,\,2}$ coefficients are assumed constant in the neighborhood of the contact point O.

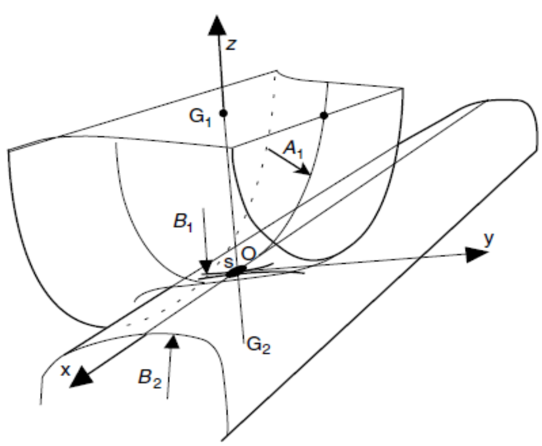

Hertzian contact: the railway case.

Figure 3.3: Hertizian wheel rail contact

Wheel $\frac{d^2 z_1}{dx^2} = 2A_1 \approx \frac{1}{r_n}$ 3.2a

Rail $\frac{d^2 z_1}{dy^2} = 2B_1 \approx \frac{1}{R_{wx}}$ 3.2b

In the railway case, the curvature A_2 is generally neglected as the rail is straight the radius is infinite: B_1 and B_2 are deduced from the transverse profiles, A_1 from r_n, the normal radius of the wheel, itself deduced from r_o, the rolling radius of the wheel. The transversal radii of curvatures of wheel and rail profiles at the contact region are represented by $R_{wx} and\ R_{rx}$ respectively.

$$\frac{1}{r_n} = \frac{cos\gamma}{r_0} \quad 3.3$$

Note that: the r_o value at the contact point is slightly different between the tread and the flange, but this variation (+10 to +15 mm) is a second order compared to the cos γ influence.

Before being loaded, the vertical relative distance d(x,y) between the two bodies can be written:

$$z_1 + z_2 = d = \mathrm{A}\, x^2 + By^2 \quad 3.4a$$

$$\mathrm{A}=\frac{1}{2r_n} \text{ and } \mathrm{B}=\frac{1}{2}\left(\frac{1}{R_{wx}} + \frac{1}{R_{rx}}\right) \quad 3.4b$$

A and B being strictly positive.

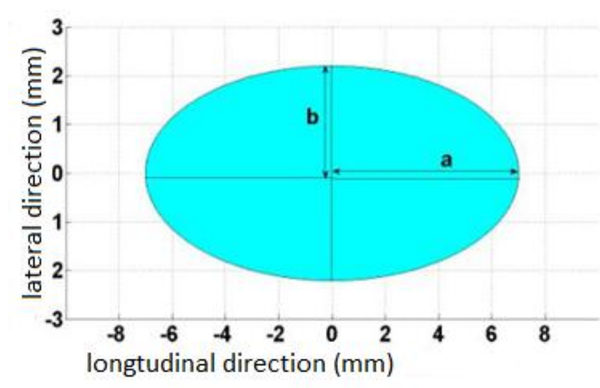

Figure 3.4: Hertizian elliptical contact patch model

Conventionally, ‘a’ is the ellipse longitudinal semi axis in the x direction and ‘b’ is in the transversal y direction. The A/B and b/ a ratios vary in the same way: if A $>$ B, then b $> a$.

The equality A/B =1 leads to a circular contact patch: a = b.

The traditional calculation is based on the determination of the semi axis ratio: g< 1, (g = b/ a or a /b), function of B/A by using an intermediate parameter, the angle θ defined as:

$$\cos\theta = \frac{|B-A|}{B+A} \qquad 3.5$$

The practical values of the semi-axis a and b, and δ the reduction of the distance between the bodies' centers are given by:

$if\ a > b$:

$$a = m\left(\frac{3}{2}N\frac{1-\text{v}^2}{E}\frac{1}{A+B}\right)^{1/3} \qquad 3.6a$$

$$b = n\left(\frac{3}{2}N\frac{1-\text{v}^2}{E}\frac{1}{A+B}\right)^{1/3} \qquad 3.6b$$

$$\delta = r\left(\left(\frac{3}{2}N\frac{1-\text{v}^2}{E}\right)^2(A+B)\right)^{1/3} \qquad 3.6c$$

With E being the Young's modulus and v the Poisson's ratio, assuming the same material for the rail and the wheel. N is the vertical load applied normal to the contact patch.

m, n, and r are nondimensional coefficients tabulated as a function of the ratio g = n/m or the angle θ.

The relationship between A/B and the constants m, n, and r are specified on [Iwnicki S. ed., 2006]

Table: 3.1: Hertz Coefficients for θ =0 to 180^0(m and r values relative to A/B or b/ a)

$\theta°$	0	5	10	30	60	90	120	150	170	175	180
A/B	0	0.0019	0.0077	0.0717	0.3333	1	3.0	13.93	130.6	524.6	∞
$b/a = n/m$	0	0.0212	0.0470	0.1806	0.4826	1	2.0720	5.5380	21.26	47.20	∞
m	∞	11.238	6.612	2.731	1.486	1	0.7171	0.4931	0.311	0.2381	0
r	0	0.2969	0.4280	0.7263	0.9376	1	0.9376	0.7263	0.4280	0.2969	0

$n = 3E\text{-}05\theta^2 + 0.00450\theta + 0.334$ 3.7a

$m = 62.190\theta\text{-}0.914$ 3.7b

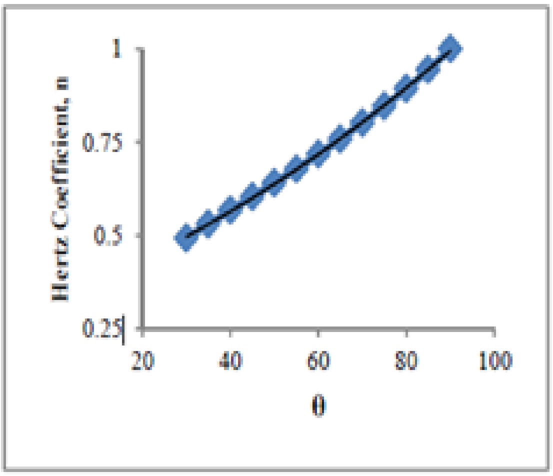

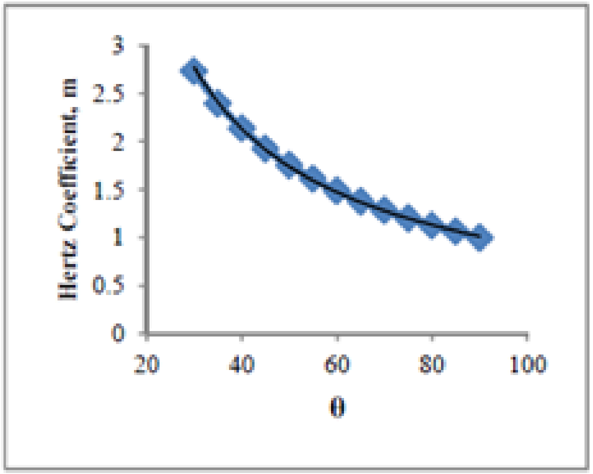

a) b)

Figure 3.5: Graph showing relation between n and m coefficients with Θ

πab being the surface area of the ellipse, it can be expressed as a function of:

$$ab = mn\left(\frac{3}{2}\frac{1-\text{v}^2}{E}\frac{1}{A+B}\right)^{2/3} N^{2/3} \qquad 3.8$$

The calculation of the contact areas requires knowledge of some geometric constants used in the above formulation. With respect to wheel-rail configuration, the following curvature combinations are related as:

$$\text{A+B}=\frac{1}{2}\left(\frac{1}{R_{11}}+\frac{1}{R_{12}}+\frac{1}{R_{22}}+\frac{1}{R_{21}}\right) \qquad 3.9a$$

$$\text{B-A}= \frac{1}{2}\left[\left(\frac{1}{R_{11}}-\frac{1}{R_{12}}\right)^2+\left(\frac{1}{R_{22}}-\frac{1}{R_{21}}\right)^2+\ 2\left(\frac{1}{R_{11}}-\frac{1}{R_{12}}\right)\left(\frac{1}{R_{22}}-\frac{1}{R_{21}}\right)\ cos2\gamma\right]^{1/2} \qquad 3.9b$$

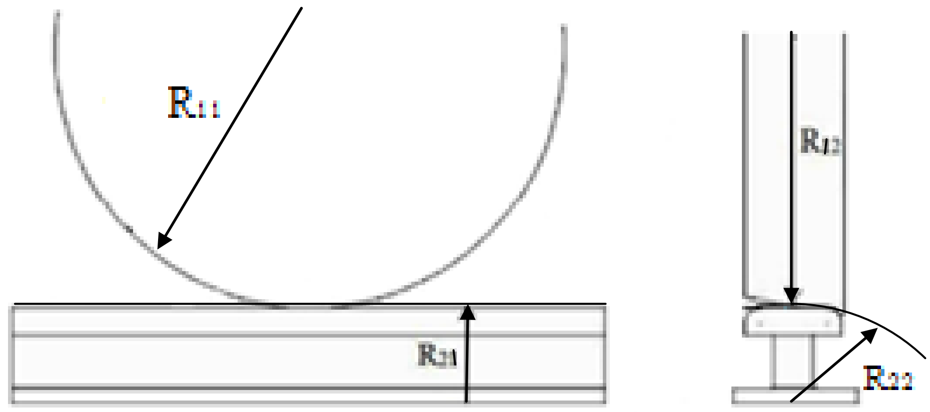

Figure 3.6: Radius of curvatures of wheel and rail profiles.

Figure Wheel-Rail Configuration showing different principal relative radii of curvature

Where,

R_{11}: The rolling radius of curvature of the wheel.

R_{12}: The radius of the wheel profile, which goes to infinity for a conical wheel.

R_{21}: The radius of the runway which is infinity in this case.

R_{22}: The radius of curvature of the rail in the plane of cross section. And

γ: conicity (wheel taper angle)

3.2.1 Convexity, Concavity and Radius Sign

The sign of each radius is important, because one of the calculation method uses A - B and A +B values to determinate the shape of the ellipse. Each radius is positive if the curvature centre is inside the body. Most of the time, the wheel rolling radius and the rail transverse radius are positive (convex). However, the wheel transverse radius at the contact point can be positive (convex) or negative (concave).

3.2.2 Particular Case: 2D Contact

When the wheel and the rail are conformal, they have the same transversal curvature value with opposite sign, giving B = 0: In this case, the contact is described as 2D, the 3D model being the classical ellipse.

3.2.3 Contact Pressure

With an elliptical pressure distribution, the mean pressure being N/πab; the maximum pressure will be simply:

$$p_o=\frac{1.5\mathrm{N}}{\pi ab} \qquad 3.10$$

In the railway field, the maximum contact pressure is frequently over 1000 MPa. This value is over the elastic limit of most steels, but the compression state is more complex than a simple tensile test and the elastic limit is not reached. The determination of the plastification (which is a limit of the Hertzian hypothesis) must be calculated with a criterion based on the hydrostatic stress (Von Mises…).

Table 3.2 Shows values of Hertz coefficients (for A/B< 1)

$\theta°$	**90**	**80**	**70**	**60**	**50**	**40**	**30**	**20**	**10**	**0**
$g = n/m$	1	0.7916	0.6225	0.4828	0.3652	0.2656	0.1806	0.1080	0.0470	0
m	1	1.128	1.285	1.486	1.754	2.136	2.731	3.816	6.612	∞
n	1	0.8927	0.8000	0.7171	0.6407	0.5673	0.4931	0.4122	0.3110	0
r	1	0.9932	0.9726	0.9376	0.8867	0.8177	0.7263	0.6038	0.4280	0

3.2.4 Analytical Approximation of the Tables

Rather reliable expressions of the n/m and mn values function of A/B (0, ∞) can be found with:

$$\boldsymbol{\frac{b}{a}=\frac{n}{m}\approx\left(\frac{A}{B}\right)^{0.63}} \qquad \mathbf{3.11}$$

3.2.5 Conicity (γ)

There is such a large set of wheel profiles that the main cone of the wheel is not able to describe the wheel – rail contact; for a large part of the time, the contact is not on the conical part of the wheel. The mean value is considered to be the conicity. Its calculation does consider the wheel profile, but also the rail profile and the flange way clearance.

With a perfectly conical wheel, the contact place on the rail appears to be the point with the same slope as on the wheel, measured in the YZ plane.

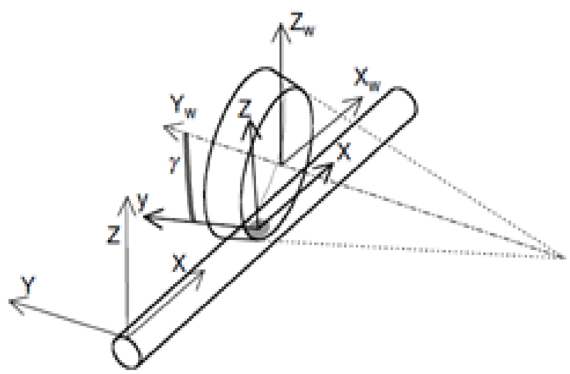

Figure 3.7: Shows contact of a perfectly conical wheel on cylindrical rail.

3.3 Tangential Contact Forces (The Tangent Problem)

3.3.2. Definition of Creepages (ξ)

The simplest theory of rolling is that in which wheel and rail are considered as rigid and the contact is governed by Coulomb's friction law. In such a theory the circumferential velocity of the wheel and the translational velocity of the wheel over the rail are equal unless the tangential force is saturated. Since the contact takes place at a single point, the forces transmitted are concentrated forces. However, as soon as one wishes to consider frictional losses in the driving wheel of the locomotive, vehicle dynamics, strength, and fatigue calculations and wear phenomena, this simple hypothesis is too crude. Indeed, in vehicle dynamics the small velocities that actually occur in wheel-rail contact are important; in strength and fatigue calculations one cannot have concentrated forces; and in friction and wear calculations the slip-force product is essential.

The following relative motions can be defined:

V_T translational velocity

V_C circumferential velocity

ξ longitudinal creepage

η lateral creepage

φ rotational creepage

Ω_x rotation of the wheel around x-axes

Ω_y rotation of the wheel around y-axes

Ω_z rotation of the wheel around z-axes

α the yaw angle

γ conicity

y lateral displacement of the wheelset

r_o rolling radius of the wheel.

- A displacement parallel to the *z* axes is given by δ. Such displacement is called compression if $\delta < 0$, and loss of contact if $\delta > 0$.
- The tangential velocities along x and y axes called the tangential velocities can be defined as :

$$V_{roll,x} = -\frac{1}{2}(V_{T,x} + V_{C,x}) \quad 3.12a$$

$$V_{roll,y} = -\frac{1}{2}(V_{T,y} + V_{C,y}) \quad 3.12b$$

- The total rolling velocity is given by:

$$V_{roll} = (V^2_{roll,x} + V^2_{roll,y})^{1/2} \quad 3.13$$

We can assume that the x component is much larger than the y component (i.e $V_{roll} \approx V_{roll,x}$)

The creep velocity divided by the rolling velocity is called creepage. Correspondingly, we have three types of creepages

Longitudinal creepage:

$$\xi = V_x/V_{roll} = (V_{T,x} - V_{C,x})/ V_{roll} \quad 3.14a$$

$$\approx \Delta r/r_o$$

$= \gamma y$,which is opposite in sign for the left and right wheels.

$$\xi_l = \gamma y \quad , \quad \xi_r = -\gamma y \quad 3.14b$$

Lateral creepage:

$$\eta = V_y / V_{roll} = (V_{T,y} - V_{C,y}) / V_{roll} \qquad 3.15$$

The lateral creepage in quasi-static conditions, with small creepages, is simply the yaw angle common to the two wheels:

$$\eta = -\alpha$$

Rotational creepage:

The difference of rotation around x and y axes are called rolling

i.e $$\Omega_x = \Omega_{T,x} - \Omega_{C,x} \qquad 3.16a$$

$$\Omega_y = \Omega_{T,y} - \Omega_{C,y} \qquad 3.16b$$

The difference of rotation around the z axes is called spin

i.e $$\Omega_z = \Omega_{T,z} - \Omega_{C,z} \qquad 3.16c$$

The spin divided by the rolling velocity is called spin creepage (rotational creepage)

$$\varphi = \Omega_z / V_{roll} = (\Omega_{T,z} - \Omega_{C,z}) / V_{roll} \qquad 3.17$$

Spin creepage, or spin for short, consists of two parts. The first results from the velocity of the Yaw angle α; the second is a consequence of conicity. Spin creepage due to conicity is called Camber in the automotive industry Indeed, there is a component of rotation $\Omega z = |\Omega| \sin\gamma$ about the *z* axis. Division by $V = |\Omega| r_o$ yields the camber spin $\sin \gamma / r_o$.

Therefore the total spin is:

$$\varphi = -\frac{\alpha}{V} + \frac{\sin \gamma}{r_o} \qquad 3.18$$

When creepages and spin creepage are known, we can calculate the contact forces.

3.3.3 Tangent Forces: Rolling Friction Simple Models

In the contact coordinate systems, the forces are denoted:

- N for the normal forces
- F_x for the longitudinal creep force
- F_y for the lateral creep force in the contact plane

The F_y forces must be projected on the track plane Y and summed to give the guiding force

In the case of a Hertzian contact, the creep forces are a function of the relative speeds between rigid bodies near the contact point, the creepages. The general expression of the creep forces takes into account stiffness coefficients c_{ij} expressed in the linear theory of Kalker by:

$$F_x = -G\, ab\, c_{11}\, \xi \qquad 3.19a$$

$$F_{y,yaw} = -G\, ab\, c_{22}\, \eta \qquad 3.19b$$

$$F_{y,spin} = -G\, ab\, c_{23} c\, \varphi \quad \text{where } c=\sqrt{ab} \qquad 3.19c$$

where G is the material shear modulus (steel in the railway case);$\pi\, ab$ is the contact ellipse surface; and c_{ij} are the coefficients (kalker's coefficients).

Kalker's Coefficients C_{ij}

The c_{ij} coefficients are a given function of the b/a ratio of the ellipse (Table 3.3). Their values are not far from π for $\frac{b}{a}$ close to 1 (see Kalker's tables). Initially, Carter uses the value π. In the bibliography, the c_{11} and c_{22} values are given for Poisson's ratio values 0 or 0.25 or 0.5. The typical value of steel is close to 0.27 and the tables must be interpolated.

A polynomial fit is proposed by:

$$c_{11}=3.2893+\frac{0.975}{b/a}-\frac{0.012}{(b/a)^2} \qquad 3.20a$$

$$c_{22}=2.4014+\frac{1.3179}{b/a}-\frac{0.02}{(b/a)^2} \qquad 3.20b$$

$$c_{23}=0.4147+\frac{1.0184}{b/a}+\frac{0.0565}{(b/a)^2}-\frac{0.0013}{(b/a)^3} \qquad 3.20c$$

Table 3.3:Kalker’s coefficient tables (from [Iwnicki S. ed, 2006])

	g	C_{11}			C_{22}			$C_{23} = -C_{32}$			C_{33}		
		v = 0	1/4	1/2	v = 0	1/4	1/2	v = 0	1/4	1/2	v = 0	1/4	1/2
	0.0	$\pi^2/4(1-\sigma)$			$\pi^2/4 = 2{,}47$			$\pi\sqrt{g}/3$	—	—	$\pi^2/16(1\text{-}\sigma)g$		
a/b	0.1	2.51	3.31	4.85	2.51	2.52	2.53	0.334	0.473	0.731	6.42	8.28	11.7
	0.2	2.59	3.37	4.81	2.59	2.63	2.66	0.483	0.603	0.809	3.46	4.27	5.66
	0.3	2.68	3.44	4.80	2.68	2.75	2.81	0.607	0.715	0.889	2.49	2.96	3.72
	0.4	2.78	3.53	4.82	2.78	2.88	2.98	0.720	0.823	0.977	2.02	2.32	2.77
	0.5	2.88	3.62	4.83	2.88	3.01	3.14	0.827	0.929	1.07	1.74	1.93	2.22
	0.6	2.98	3.72	4.91	2.98	3.14	3.31	0.930	1.03	1.18	1.56	1.68	1.86
	0.7	3.09	3.81	4.97	3.09	3.28	3.48	1.03	1.14	1.29	1.43	1.50	1.60
	0.8	3.19	3.91	5.05	3.19	3.41	3.65	1.13	1.25	1.40	1.34	1.37	1.42
	0.9	3.29	4.01	5.12	3.29	3.54	3.82	1.23	1.36	1.51	1.27	1.27	1.27
b/a	*1.0*	*3.40*	*4.12*	*5.20*	*3.40*	*3.67*	*3.98*	*1.33*	*1.47*	*1.63*	*1.21*	*1.19*	*1.16*
	0.9	3.51	4.22	5.30	3.51	3.81	4.16	1.44	1.59	1.77	1.16	1.11	1.06
	0.8	3.65	4.36	5.42	3.65	3.99	4.39	1.58	1.75	1.94	1.10	1.04	0.954
	0.7	3.82	4.54	5.58	3.82	4.21	4.67	1.76	1.95	2.18	1.05	0.965	0.852
	0.6	4.06	4.78	5.80	4.06	4.50	5.04	2.01	2.23	2.50	1.01	0.892	0.751
	0.5	4.37	5.10	6.11	4.37	4.90	5.56	2.35	2.62	2.96	0.958	0.819	0.650
	0.4	4.84	5.57	5.57	4.84	5.48	6.31	2.88	3.24	3.70	0.912	0.747	0.549
	0.3	5.57	6.34	7.34	5.57	6.40	7.51	3.79	4.32	5.01	0.868	0.674	0.446
	0.2	6.96	7.78	8.82	6.96	8.14	9.79	5.72	6.63	7.89	0.828	0.601	0.341
	0.1	10.7	11.7	12.9	10.7	12.8	16.0	12.2	14.6	18.0	0.795	0.526	0.228

3.3.4 Discretised Ellipse: FASTSIM from Kalker

Kalker developed a FE approximation of the elliptical contact patch using a program FASTSIM, He divided the elliptical contact surface into independent longitudinal parallel strips see figure (3.8) some of his assumption is common to Hertz.

- The contact surface is elliptic and flat, the pressure p_z is an ellipsoid
- The creepages are estimated at the ellipse centre
- Kalker’s coefficients c_{ij} are constant everywhere in the ellipse, their values are deduced from A/B or b/a
- The elliptic contact surface is divided into independent longitudinal parallel strips of length a_i and width Δy_i
- All the strips are divided into the same number of elements; the stress calculation begins from the leading edge, from element to element
- The method is simplified: a local deformation corresponds to a local force
- The saturation is calculated independently for each element loaded by the normal force n_{ij}. Practically, the surface is described by a grid separating parallel strips in the direction of rolling.

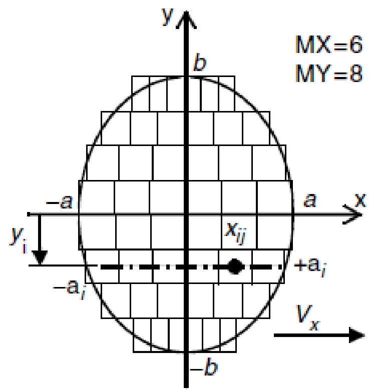

Figure 3.8: Strips and elements discretization with FASTSIM

Stresses:

The unsaturated stress distribution in the x and y directions is the following

$$P(x,y_i)=\left(\frac{\xi}{L_1} - yi\ \frac{\varphi}{L_3}\right)(x- a_i) \qquad 3.21$$

The first term represents the mean rigid longitudinal slip, and the second term is the spin effect as a local rigid slip at the point (x, y) in the strip, a_i being the leading edge of this strip.

$$P(x,y)= \frac{\eta}{L_2}(x- a_i) + \frac{\varphi}{2L_3}(x^2- a_i^2) \qquad 3.22$$

Where L_1, L_2, L_3 are the elasticity coefficients (or flexibilities) of the contact:

$L_1 =\frac{8a}{3c_{11}G}$ $\qquad$ $L_2 =\frac{8a}{3c_{22}G}$ $\qquad$ $L_3 = \frac{\pi a\sqrt{a/b}}{4c_{23}G}$

Linear Contact Forces, Elastic Coefficients:

The contact forces are the integral distributions of the surface stresses. When there is no saturation:

$$F_x = -\iint p_x(x)dxdy = \frac{-8a^2b\xi}{3L_1} \qquad 3.23a$$

$$F_y = -\iint p_y(x)dxdy = \frac{-8a^2b\eta}{3L_2} - \frac{\pi a^3 b\varphi}{4L_3} \qquad 3.23b$$

Note that: Typical values of the creepages for straight track rolling are $\xi, \eta \approx 0.5\%$ and $\varphi \approx 0.01\%$as specified on [kalker, 1990]

Stress

Pressure distribution is semi-ellipsoidal, therefore for a total load N the mean contact stress, p_m, is given by, p_m=$\frac{N}{\pi ab}$ and the maximum contact stress is given by:

$$p_o = \frac{3N}{2\pi ab} = 1.5 p_m \quad 3.24$$

The pressure distribution within the contact ellipse will be given by:

$$p(x, y) = p_o \sqrt{1 - \frac{x^2}{a^2} - \frac{y^2}{b^2}} \quad 3.25$$

The principal direct stresses acting along the z,x,y axes at or below ,the contact center are: $\sigma_x, \sigma_y, and\ \sigma_z$.the shear stress acting along these axes at or below the contact center are zero. The principal shear stresses act on the planes bisecting the angle between the z,x,y planes .Their magnitude by Tresca's criterion is given by:

$$\frac{(\sigma_z - \sigma_x)}{2} \quad \text{in the zx plane} \quad 3.26a$$

$$\frac{(\sigma_x - \sigma_y)}{2} \quad \text{in the xy plane} \quad 3.26b$$

$$\frac{(\sigma_y - \sigma_z)}{2} \quad \text{in the yz plane} \quad 3.26c$$

For an elliptical contact, direct stresses along the principal planes /axes at the center of contact surface are:

$$\sigma_z = p_o \quad 3.27a$$

$$\sigma_x = 2\nu p_o + (1 - 2\nu).(\frac{b}{\{a+b\}}) \quad 3.27b$$

$$\sigma_y = 2\nu p_o + (1 - 2\nu).(\frac{a}{\{a+b\}}) \quad 3.27c$$

The maximum shear stress is given by,

$$\tau_{\max} \approx \frac{p_o}{3} = \frac{N}{2\pi ab} \quad 3.28$$

As the principal shear stress in the plane of deformation $\tau_1 = p_o(\frac{F}{N})$=K,then material throughout the width of the contact surface will begin to yield where F is the tangential creep force.

3.3.5. Tresca's and Von Mises criteria of plastic deformation.

With complex stress systems, the state of stress can always be described in terms of the three principal stresses $\sigma_1, \sigma_2, and\ \sigma_3$. Yield criteria then define conditions where plastic behavior is initiated for any combination of these stresses; only sudden initiation of yield is considered.
Two criteria are commonly used: Tresca's and Von Mises

The Tresca criterion states that "plastic behavior occurs when the maximum shear stresses reach a critical value.
If the three principal stresses are $\sigma_1, \sigma_2, and\ \sigma_3$ with $\sigma_1 > \sigma_2 > \sigma_3$ then,

The maximum shear stress = $\frac{(\sigma_1 - \sigma_2)}{2}$ 3.29

For uniaxial tension (in one direction) $\sigma_2 = \sigma_3 = 0, and\ \sigma_1 = Y$, the yield stress in simple tension, then the maximum shear stress becomes $\frac{\sigma_1}{2}$ (i.e $\tau_1 = \frac{\sigma_1}{2} = \frac{Y}{2}$)

For pure shear where k is the yield stress in simple shear $\sigma_2 = 0, and\ \sigma_1 = -\sigma_3 = k$,then the maximum shear stress becomes σ_1 (i.e $\tau_1 = \sigma_1 = k$)
Thus the Tresca criterion can be generalized as:

$$\{|\sigma_1 - \sigma_2|, |\sigma_1 - \sigma_3|, |\sigma_2 - \sigma_3|\}_{max} = 2k = Y \quad 3.30$$

Von Mises criterion takes into account the fact that metals cannot be compressed in all directions and therefore the hydrostatic component $\sigma_h = (\sigma_1 + \sigma_2 + \sigma_3)/3$ must be considered. Thus the effective principal stresses are: $(\sigma_1 - \sigma_h)$, $(\sigma_2 - \sigma_h), and\ (\sigma_3 - \sigma_h)$ .The criterion states that "deformation occurs when this reaches a critical value" that is :

$$(\sigma_1 - \sigma_h)^2 + (\sigma_2 - \sigma_h)^2 + (\sigma_3 - \sigma_h)^2 = [(\sigma_1 - \sigma_2)^2 + (\sigma_2 - \sigma_3)^2 + (\sigma_3 - \sigma_1)^2]/3 = \text{constant} \quad 3.31$$

Again considering the case of uniaxial tension ,where $\sigma_2 = \sigma_3 = 0, and\ \sigma_1 = Y$, the constant becomes $\frac{2}{3}(Y)^2$
From the case of pure shear, $(\sigma_2 = 0, and\ \sigma_1 = -\sigma_3 = k)$ the constant becomes $2(k)^2$
Therefore for Von Mises case

$$k=0.58Y \qquad 3.32$$

$$[(\sigma_1-\sigma_2)^2+(\sigma_2-\sigma_3)^2+(\sigma_3-\sigma_1)^2] = 2(Y)^2 = 6K^2 \qquad 3.33$$

This differs slightly from Tresca. Although refined experiments with ductile metals tend to support Von Mises, as the difference is small and most metals are not fully isotropic, Tresca is usually used for algebraic simplicity. [Jonson, 1985]

3.4 Prediction of wheel fatigue

There are a multitude of different numerical models to analyze wheel fatigue reported in the literature. Here, the presentation will focus on general stress fatigue in the wheel rim. Only some selected models are presented which have the benefit of being described in analytical form.

3.4.1 Subsurface-initiated rolling contact fatigue

To facilitate the prediction of subsurface-initiated RCF, we will distinguish between the cases of shallow initiation (say, from some 4 mm to some 10 mm below the wheel tread) and deep initiation (say, at some 10-25 mm below the tread).

For the shallow cracks we presume fatigue initiation to be related to the magnitude of the shear stress. Assuming Hertzian contact conditions the maximum shear stress will occur some millimeters below the tread surface and have an approximate magnitude of

$$\tau_{\max} \approx \frac{p_o}{3} = \frac{N}{2\pi ab} \qquad 3.34$$

Here, p_o is the peak normal contact pressure, N the total normal contact load and a and b the semi-axes of the Hertzian contact patch.

Since the state of stress in the wheel rim is multiaxial, an equivalent stress criterion will be employed to quantify the fatigue impact. Here, we use a multiaxial fatigue criterion (Dang Van *et al.*, 1989), which can be expressed as:

$$\sigma_{EQ} = \tau_a + a_{DV}\sigma_h \qquad 3.35a$$

a_{DV} is a material parameter that may be evaluated as:

$$a_{DV}=\frac{3\tau_e}{\sigma_e}-\frac{3}{2} \tag{3.35b}$$

Where τ_e is the fatigue limit in alternating shear, and σ_e is the fatigue limit in rotating bending

$\sigma_h = \frac{(\sigma_x+\sigma_y+\sigma_z)}{3}$ is the hydrostatic stress (positive in tension) .

For wheel-rail contact conditions there is a pulsating shear stress evolution on the shear plane experiencing the highest 'amplitude'. The shear stress 'amplitude' τ_a, is for this case half of the maximum shear $\tau_{\max}$.

$$\tau_a = \frac{\tau_{\max}}{2} = \frac{N}{4\pi ab} \tag{3.36}$$

If additional frictional loading of moderate magnitude is applied, the maximum shear stress may be estimated at:

$$\tau_{\max} = \frac{N}{2\pi ab}(1+f^2) \tag{3.37}$$

Here $f = \frac{\sqrt{F_x{}^2+F_y{}^2}}{N}$ where F_x and F_y are tangential forces.

Combining Eqs (3.35a) and (3.37), the equivalent stress can be expressed as:

$$\sigma_{EQ} = \frac{N}{4\pi ab}(1+f^2)+a_{DV}\sigma_{h,res} \tag{3.38}$$

Where $\sigma_{h,res}$ is the hydrostatic part of the residual stress.

Fatigue is predicted to occur if $\sigma_{EQ} > \tau_e$ where τ_e is the fatigue limit in shear, which is roughly $\frac{\sigma_u}{3}$ where σ_u, is the tensile fracture stress of the material.

As seen above, the size of the contact patch *(πab)* will influence the magnitude of the fatigue impact (σ_{EQ}).In addition, the shape of the contact patch will have an influence. In wheel-rail contact, the patch is normally elongated *(a>b)* in the rolling direction.

If we look at RCF initiation deeper into the wheel rim, interfacial wheel-rail friction and the size and shape of the contact patch will have less influence. Instead, the magnitude of the total contact load and the occurrence of material defects will be the main influential factors which will not be presented in this paper.

3.4.2 Surface-initiated rolling contact fatigue

If the assumed main material response is in the plastic shakedown stage, a LCF criterion that is able to account for the multiaxial state of stress and strain should be used. An example is given in [Jiang and Sehitoglu, 1999] where a fatigue parameter *FP* is defined as

$$FP = \Delta\varepsilon . (\sigma_{max}) + J . \Delta \vartheta \, \Delta\tau \qquad 3.39$$

The criterion is evaluated for a material plane where $\Delta\varepsilon$ is the range of the normal strain acting on the plane, σ_{max} =max (σ_{max},0), withσ_{max}, being the largest normal stress on the plane. Further, J is a material parameter, $\Delta \vartheta$ the range of the (engineering) shear strain and $\Delta\tau$ the range of the shear stress. Note that the evaluation of $\Delta \vartheta$ and $\Delta\tau$ needs to account for the fact that these are vector quantities. The fatigue life ***N*** can then be evaluated by an extension of traditional (uniaxial) LCF predictive models as:

$$FP = \frac{\sigma_f'^{2}}{E} (2N_f)^{2b} + \varepsilon_f'(2N_f)^{b+c} \qquad 3.40$$

where E is the elasticity modulus, and σ_f', ε_f',b**,** and c are additional material parameters.
If, instead, ratcheting is considered as the dominating damage mechanism, a ratcheting criterion [Kapoor, 1994] may be employed:

$$\Sigma\varepsilon_i = \varepsilon_c \qquad 3.41$$

Here ε_i is the current strain increment and ε_c**,** the fracture strain. When applied to surface-initiated RCF in railway wheels, $\varepsilon_i$needs to account for the multiaxial state of strain. An approach to this is to define an effective strain increment in line with the use of equivalent stresses discussed in [Kapoor, 1994].

The main cause of global plastic deformation of the surface material is the applied interfacial shear stress between the wheel tread and the rail. As the frictional loading increases from zero, the depth of the location of the maximum shear stress decreases (and the magnitude increases) slightly as compared to pure rolling. At traction coefficient of roughly $f = 0.3$ the location of maximum shear stress will jump to the surface and its magnitude increases strongly with increasing interfacial friction. In addition, the shear stress magnitude decreases rapidly with depth.

The shear stress (traction) *q(x,y)* in the wheel-rail interface is presumed to be proportional to the contact

Pressure via the traction coefficient f:

$$q(x, y) = f.p(x, y) \tag{3.42}$$

The peak traction will thus be: $q_o = fp_o$

Where p_o is the peak contact pressure, which according to Hertzian theory is expressed as

$p_o=\frac{3N}{2\pi ab}$

A criterion for surface plasticity may be expressed as:

$$q_o = k \tag{3.43}$$

Where k is the yield limit in shear of the wheel material.

A combination of Eqs (3.42) and (3.43) results in the yield criterion:

$$fp_o = k. \leftrightarrow \frac{3N}{2\pi abk} = \frac{1}{f} \tag{3.44}$$

3.4.3 Fatigue damage per cycle, D

The other parameter used to quantify the fatigue impact is the concept of fatigue damage. For one stress cycle the fatigue damage can be defined as $D=1/N_f$, where N_f is the fatigue life in terms of stress cycle for the current stress amplitude. Fatigue failure is then assumed to occur at a material point when the total accumulated amount of damage D attains the value 1(unity).

When the equivalent stress in a material point exceeds a certain value, it is postulated that fatigue damage will occur .The amount of fatigue damage that will be induced is quantified using an approach setting out from the wohler curve or (S-N) curve in short. It assumed that the equivalent fatigue limit, σ_e , corresponds to 10^6 stress cycles and that an equivalent stress level corresponding to the ultimate (equivalent strength),S_u corresponding to 10^1 stress cycles .the fatigue damage per cycle corresponding to an equivalent stress level σ_{EQ} can be expressed as :

$$D=10^{\frac{5(\sigma_e-\sigma_{EQ})}{\sigma_e-Su}-6} \qquad 3.45a$$

$$N_f=1/D \qquad 3.45b$$

Naturally more accurate results cannot be estimated using this approach since the Dang Van equivalent stress only reflects the fatigue behavior of the material for load magnitude close to the fatigue limit. The approach will however reflect the exponential growth of the fatigue damage with stress magnitude which in turn is also a function of other parameters such as the geometrical size of load contact patch.

Researches were carried out to understand and model wheel/rail wear behavior. Empirical studies, both on a full-scale laboratory test rig and in the field [McEwen and Harvey, 1986], [Pearce and Sherratt, 1990]), have shown that the wear of wheels and rails depends on the rate of dissipation of energy within the contact patch. It had been concluded that wheel wear rate could be related to the frictional energy expended through creepage in each wheel/rail contact. This can be shown to be the sum of the products of the individual creep forces, and creepages in the longitudinal and lateral directions as illustrated in [Ivan Y. Shevtsov, 2008].In most cases, the contribution from the spin term is assumed to be small and is ignored. Wheel wear is estimated using the wear index *W* that reads:

$$W = Fx * \xi + Fy * \eta \qquad 3.46$$

Where *F x* is longitudinal creep force; ξ is longitudinal creepage ; *F y* is lateral creep force; and η is lateral creepage

3.5 Theoretical results

Here, the Equations involved to calculating the contact dimension, stress, creep forces & contact parameters such as equivalent stress, fatigue damage per cycle and expected fatigue life between wheel-rail contact pair varying contact geometry are briefly illustrated. The rail used in the present study is as per Chinese national railways standard (GB 50kg) which is under operational for the track of Addis Ababa Light Rail Train. The wheel is as per international union of railway (UIC) standard.

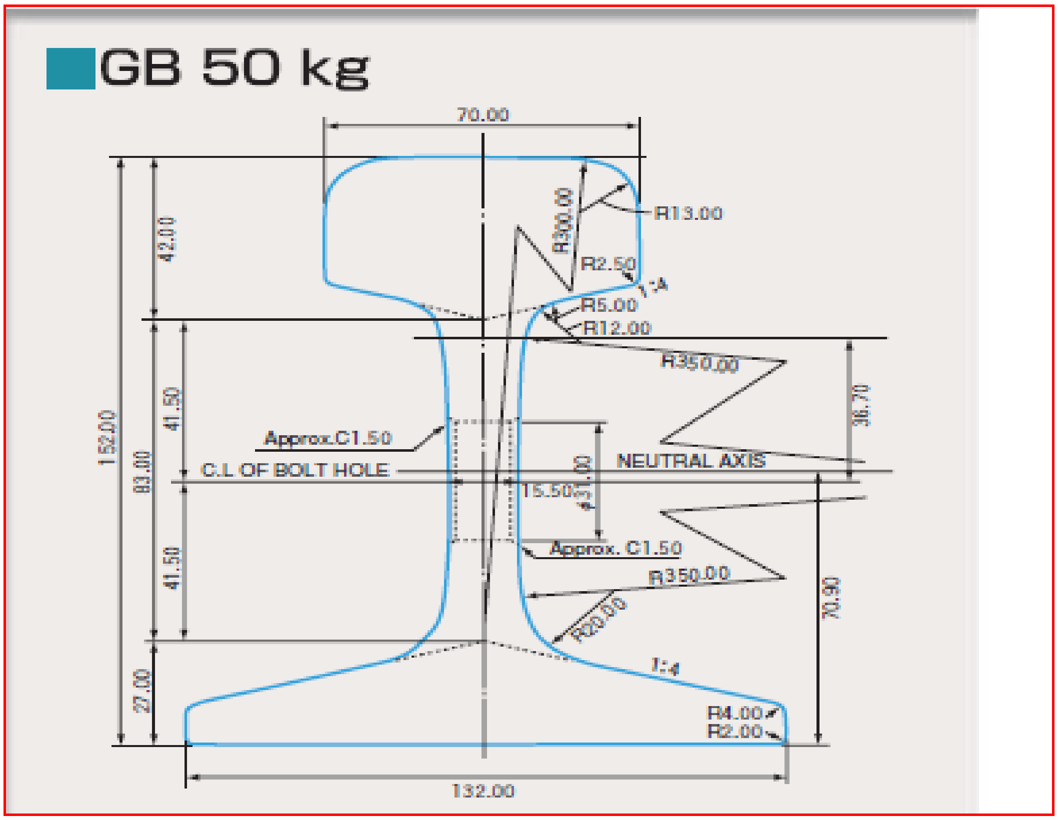

Figure 3.9: Rail profile as per Chinese national railways standard

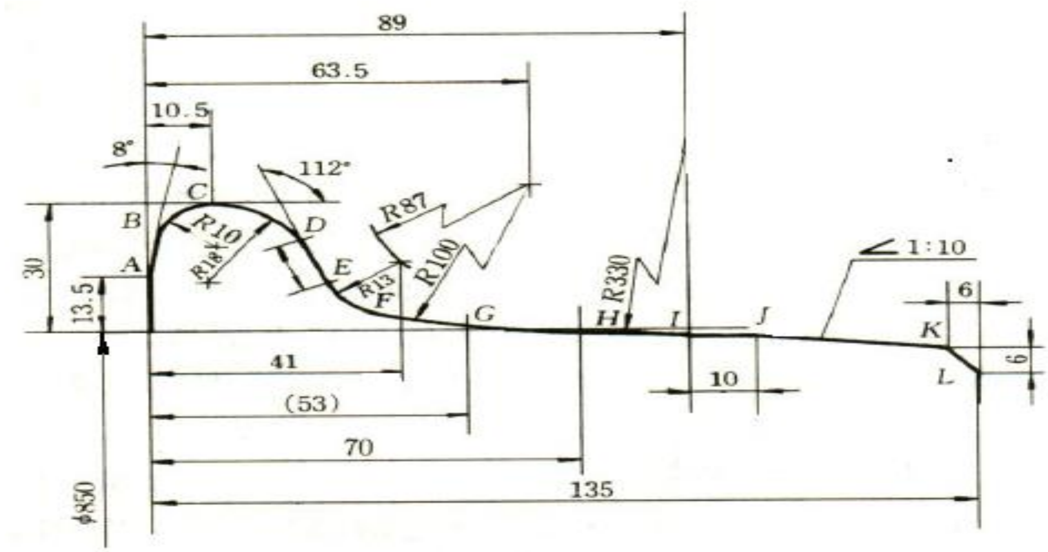

Figure 3.10: A common wheel profile for UIC standard wheels

The contact load and material properties used in the analysis are presented below:

- The contact load is taken as 90KN (9 tone).
- Maximum Acceleration:1.4m/s^2
- maximum speed =70km/h
- Youngs' modulus of elasticity E_{wheel}=E_{rail} =205 GPa,
- Poissons' ratio v=0.29
- Ultimate tensile strength ,σ_{ut} rail = σ_{ut} wheel = 1300 MPa, σ_y=750MPa for both wheel and rail
- Radius of wheel, r_o=430mm.

The variations in the geometrical parameter considered are:

- Conicity (wheel taper) , γ : from 1 in 5 to 1 in 30
- Wheel profile radius :from 300 to 360 mm and
- Rail profile radius from 280 to 330 mm.

Three geometrical conditions are selected to find numerical results using MATLAB :the variation in wheel taper (ranging from 1in 5 to 1 in 30),the variation in the transversal radius of curvature of wheel ranging from 300 to 360mm and the variation in the transversal radius of curvature of rail ranging from 280 to 330mm.For instance, as the conicity (wheel taper) varies from 1 in 20 to 1 in 25 , the normal radius of the wheel, r_n varies because r_n is a function of γ and r_o, the rolling radius of the wheel (see equation (3.3)). This in turn is responsible for the variation in the intermediate parameter , θ which is a function of the curvature of wheel and rail profiles. (See equation (3.5)).The MATLAB result for the numerical variation θ is found to be 62.2762° to 62.2876°.The values of Hertz coefficients m and n for θ=0 to 180° are given in table(3.2). The numerical values of the coefficients can be calculated from table (3.2) by interpolation. For n the numerical values vary from 0.7360 to 0.7361 and for m it varies from 1.4402 to 1.4400 . The length of diameters of the elliptical contact patch a and b are related to these coefficients as well as material parameters and the normal load N as shown in equation (3.6a)and (3.6b).The variation of a and b are calculated as 7.4584 to 7.4569mm and 3.8113 to 3.8116mm respectively. The variation in contact area can be calculated accordingly using equation (3.8) as 89.3022 to 89.2923mm^2. The maximum contact pressure p_o which depends on the size of the contact patch is also calculated as 1.5117 to 1.5119GPa. Here, it is evident that a slight variation in wheel taper results in about 0.2MPa of contact pressure. Accordingly, the variation in equivalent stress, fatigue damage per cycle, and expected stress fatigue life are determined using equations (3.38),(3.45a),(3.45b) respectively .The details of this calculations are summarized in table (3.4)

In a similar manner, the variations in the transversal radius of curvatures of wheel and rail are also investigated and summarized in table (3.5) and (3.6) respectively. In all three cases, similar formulas are used. However, the parameters that vary are different. For instance, in table(3.4) the parameter that vary is the conicity, γ and in table (3.5) and (3.6) the parameters that vary are the radius of curvature of wheel and the radius of curvature of rail respectively.

A prediction of fatigue life dependency is higher on both the radius of curvatures of wheels and the radius of curvatures of rails. For instance, a slight increase in the radius of curvatures of rails from 300 to 310mm is responsible for a change in stress fatigue life from 43996 to 49191.which is a difference of 5195 available stress fatigue life cycles.

The results obtained are tabulated below

Table 3.4: Effect of variation in Wheel Profile Taper (conicity, γ) on different contact parameters, R_{11}=430 mm, R_{12}=330 mm, $R_{21}=\infty$, R_{22}=300 mm

Wheel taper (conicity), γ	a (mm)	b (mm)	contact area(πab) mm^2	p_o (GPa)	σ_1 (GPa)	σ_2 (GPa)	σ_3 (GPa)	σ_{eq} (MPa)	Fatigue damage per cycle ($*10^{-4}$)	Expected fatigue life(Nf) ($*10^{+4}$)
1in5	7.5190	3.7975	89.7020	1.5050	1.5050	0.8730	0.8732	899.3129	0.2277	4.3915
1 in10	7.4707	3.8085	89.3840	1.5103	1.5103	0.8761	0.8763	899.2242	0.2273	4.3996
1in15	7.4616	3.8105	89.3235	1.5114	1.5114	0.8767	0.8769	899.2159	0.2273	4.4004
1in20	7.4584	3.8113	89.3022	1.5117	1.5117	0.8769	0.8771	899.2136	0.2272	4.4006
1in25	7.4569	3.8116	89.2923	1.5119	1.5119	0.8770	0.8772	899.2126	0.2272	4.4007
1in30	7.4561	3.8118	89.2869	1.5120	1.5120	0.8771	0.8772	899.2121	0.2272	4.4008

Table 3.5: Effect of variation of radius of curvatures of wheel profile on contact parameters, Wheel profile Taper (conicity, γ) =1in 20= 2.86°, R_{11} =430 mm, $R_{21}=\infty$, R_{22}=300 mm.

radius of curvature of wheel (mm)	a (mm)	b (mm)	contact area(πab) mm^2	p_o (GPa)	σ_1 (GPa)	σ_2 (GPa)	σ_3 (GPa)	σ_{eq} (MPa)	Fatigue damage per cycle ($*10^{-4}$)	Expected fatigue life Nf, ($*10^{+4}$)
300	7.4944	3.7181	87.5406	1.5421	1.5421	0.8946	0.8947	914.2056	0.3110	3.2153
310	7.4823	3.7505	88.1599	1.5313	1.5313	0.8883	0.8884	908.8917	0.2783	3.5936
320	7.4703	3.7815	88.7463	1.5212	1.5212	0.8824	0.8826	903.9040	0.2507	3.9891
330	7.4584	3.8113	89.3022	1.5117	1.5117	0.8769	0.8771	899.2136	0.2272	4.4006
340	7.4466	3.8398	89.8298	1.5028	1.5028	0.8718	0.8719	894.7948	0.2072	4.8271
350	7.4351	3.8673	90.3311	1.4945	1.4945	0.8670	0.8671	890.6248	0.1898	5.2674
360	7.4237	3.8936	90.8078	1.4867	1.4867	0.8624	0.8625	886.6835	0.1748	5.7204

Table 3.6: Effect of variation of radius of curvatures of rail profile on contact parameters, Wheel profile Taper (conicity, γ) =1in 20= 2.86°, R_{11}=430 mm, R_{12}=330 mm, R_{21}= ∞

radius of curvature of rail (mm)	a (mm)	b (mm)	contact area(πab) mm^2	p_o (GPa)	σ_1 (GPa)	σ_2 (GPa)	σ_3 (GPa)	σ_{eq} (MPa)	Fatigue damage per cycle ($*10^{-4}$)	Expected fatigue life Nf, ($*10^{+4}$)
280	7.4871	3.7376	87.9138	1.5356	1.5356	0.8908	0.8909	911.0084	0.2909	3.4379
290	7.4727	3.7752	88.6281	1.5232	1.5232	0.8836	0.8837	904.9171	0.2561	3.9054
300	7.4584	3.8113	89.3022	1.5117	1.5117	0.8769	0.8771	899.2244	0.2273	4.3996
310	7.4442	3.8458	89.9392	1.5010	1.5010	0.8707	0.8709	893.8928	0.2033	4.9191
320	7.4301	3.8789	90.5420	1.4910	1.4910	0.8649	0.8651	888.8892	0.1831	5.4622
330	7.4161	3.9107	91.1129	1.4817	1.4817	0.8595	0.8596	884.1845	0.1659	6.0276

Chapter Four

Finite Element Analysis

4.1 Introduction

The finite element method (FEM) is a numerical technique for finding approximate solutions to boundary value problems for differential equations. It uses variational methods (the calculus of variations) to minimize an error function and produce a stable solution. Analogous to the idea that connecting many tiny straight lines can approximate a larger circle, FEM encompasses all the methods for connecting many simple element equations over many small subdomains, named finite elements, to approximate a more complex equation over a larger domain. [Hrennikoff, Alexander ,1941]

According to [Matin Shahzamanian Sichani,2013] the finite element method (FEM) analysis, as illustrated in the literature review, is the ultimate available solution to the contact problems which violates the underlying assumptions of Kalker's variational method. It is not bound to half-space assumption and various material properties can be considered. Moreover, more detailed friction laws than the well-known Coulomb's law can be used. It converts the partial differential equations (PDEs) into a system of algebraic equations. To do so, the bodies under investigation, considered as a continuum, are discretized into elements with certain number of nodes. The solution to the PDE using FEM is exact at the nodes; while in between the nodes it is approximated by polynomials known as shape functions. [Matin Shahzamanian Sichani, 2013]

In order to have more accurate contact analysis, geometry profile of the rail head section and the wheel tread are very important. For this reason a standard rail as per Chinese national railways standard (GB 50kg) section profile for the rail and UIC-812-3-84 standard wheel is chosen for the task (see figure 4.1 and figure 4.2) .The part modeling and assembly of wheel and rail contact is performed in CATIA V5 R16 . Then developing finite element mesh of wheel rail contact, and all the loading and applications of the boundary conditions are all established by using ANSYS12.0 work bench.

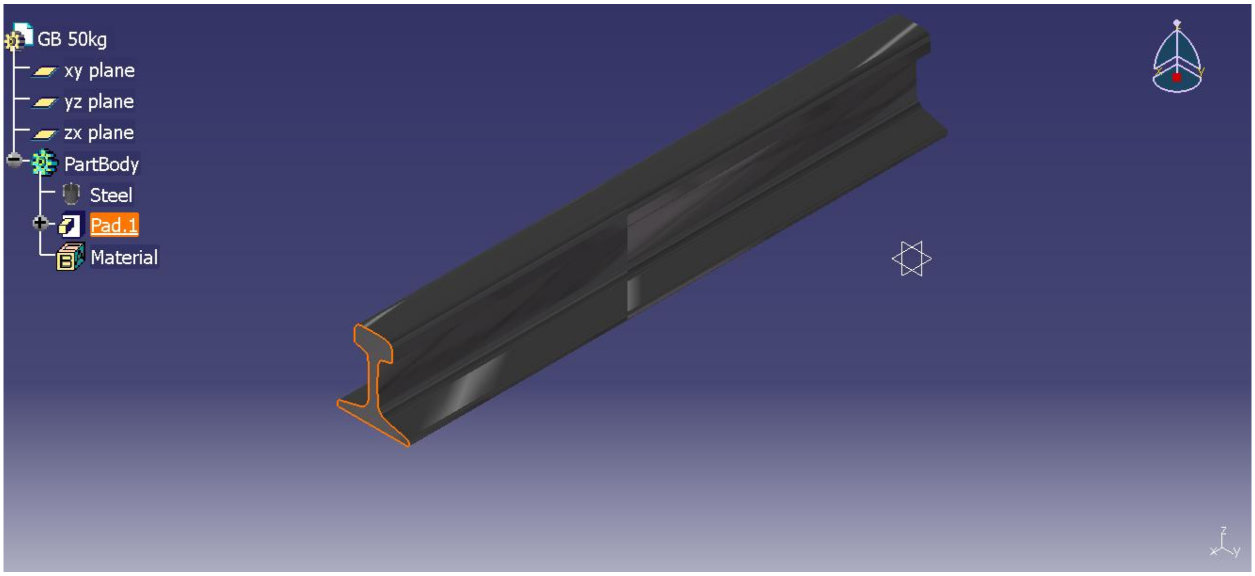

Figure 4.1: Part drawing of GB 50kg Chinese national railways standard rail

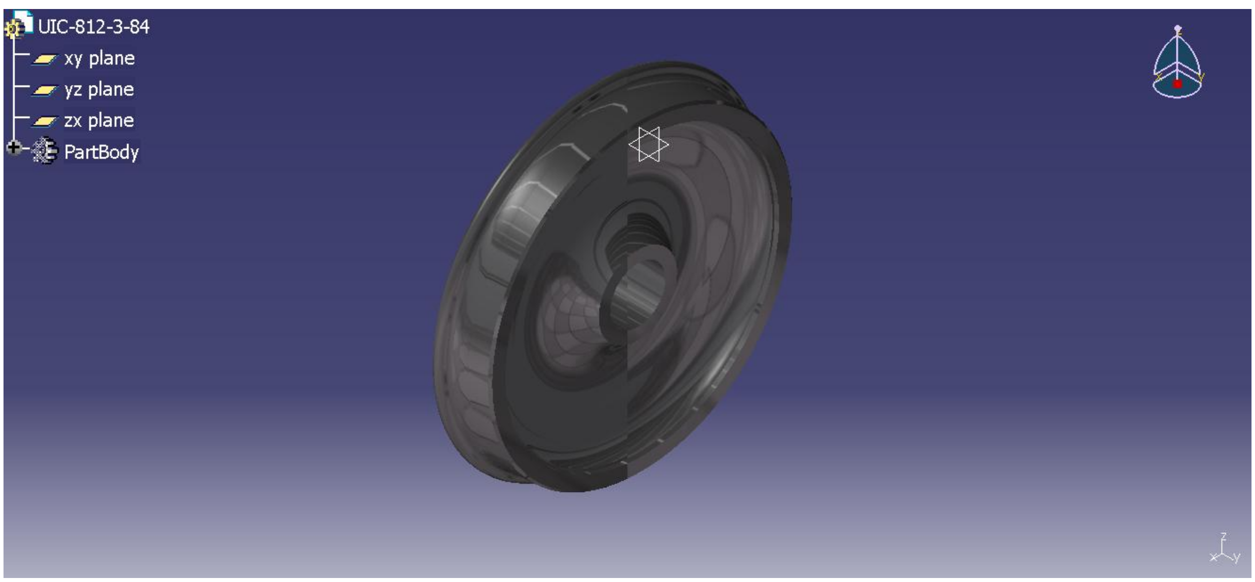

Figure 4.2: Part drawing of UIC-812-3-84 standard wheel.

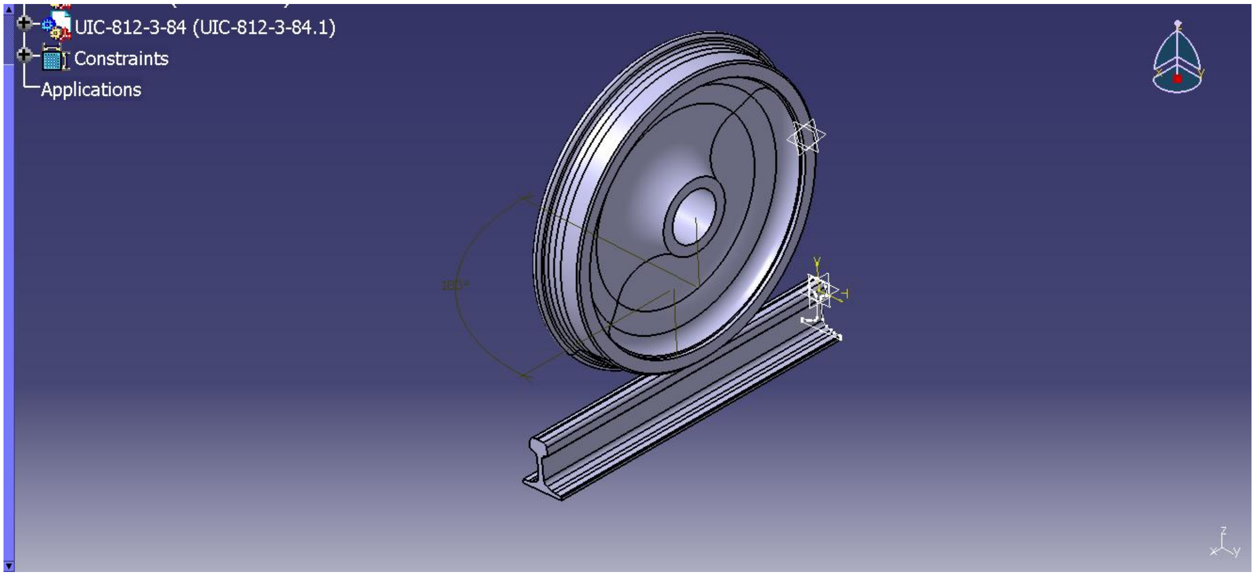

Figure4.3: UIC-812-3-84 wheel and GB 50kg standard rail contact assembly.

Meshing capability of ANSYS 12.0 Workbench is employed to generate the finite element mesh. Refinement in the contact region is performed using contact sizing option. A fine mesh with an average minimum length of 3mm is used in near contact area. Then, the meshing performed to generate the finite elements. The finite element mesh is generated in such a way that to decrease element size at the contact region (maximum stress region), increase the size of the elements when moving away from the contact region, so that there will be, More number of small size elements in the contact region and less number of elements in low stress regions respectively to reduce the computation time and computer memory requirement, within reasonable accuracy.

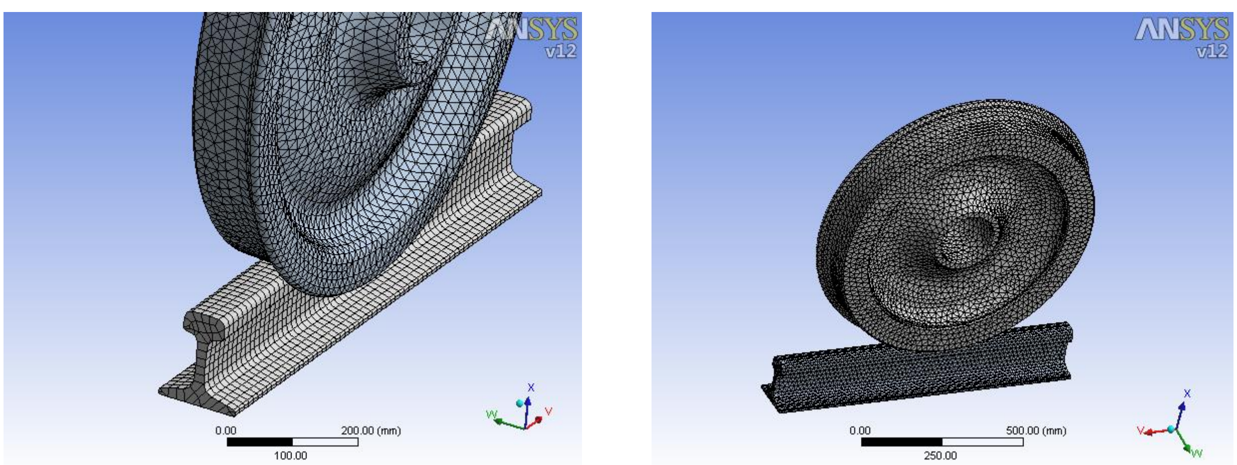

(a) (b)

Figure 4.4: (a), (b) meshed wheel - rail contact assembly in ANSYS.

The rail's length is 1m. Fixed boundary conditions (All DOF) are applied to the two area of cross section at the ends of the rail and the bottom face of the rail which is similar to the actual phenomena. Friction effect is included into material property of the contact element and a Coulomb friction model is used. The coulomb friction coefficient is assumed to be 0.3. The premium pearlitic steel with higher ultimate tensile strength (1300MPa) is used for both wheel and rail. A total wheel load of 90KN is applied at the surface of the wheel hub.

4.2 ANSYS Contact Algorism

Various algorithmic procedures have been proposed to solve contact problems in finite element analysis. Most of these procedures are based on penalty and Lagrange multiplier techniques, for enforcing the contact constraints. ANSYS uses four different contact algorithms: pure penalty method, Augmented Lagrangian method, Pure Lagrangian multiplier method and Lagrangian multiplier on contact normal and penalty on frictional direction. Augmented Lagrangian method is very similar to the penalty method except that it reduces sensitivity to contact stiffness and for this matter, for the study in hand the Augmented Lagrangian method is applied.

4.3 The Employed ANSYS Analysis Steps

In order to find numerical results from CATIA and ANSYS workbench, the steps employed are generally summarized below

a). The models for wheel and rail are generated in CATIA V5R16. Then, after assembling the model in CATIA is imported in to ANSYS Workbench 12.0 as working model.

b). Modules for automatic generation of finite element models are integrated into the model in ANSYS Workbench version 12.0, static structural analysis system. Then, the generation of finite element models is accomplished for the cycle of meshing.

c). Define material properties which are necessary to solve the problem. Here both the wheel and rail are pearlitic steel with an ultimate tensile strength of 1300MPa, yield strength 750MPa. Young's modulus of elasticity is 205 GPa.

d).To get the contact stresses the contact wizard is used in ANSYS Workbench. The contact algorithm in ANSYS Workbench computer program requires definition of contacting surface. To define a contact pair augmented Lagrangian method contact algorithm, with frictionless contact is used.

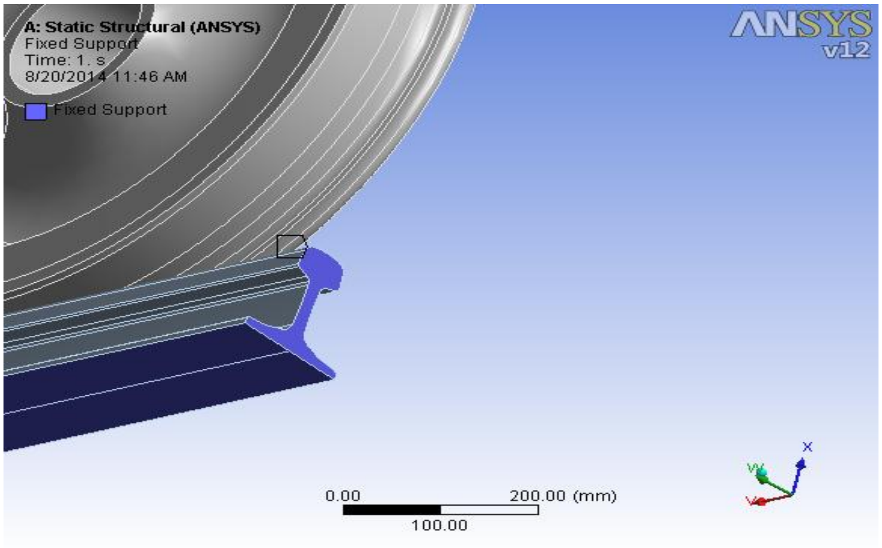

Figure 4.5: The boundary conditions of wheel rail contact assembly.

e) Fixed boundary conditions (All DOF) are applied to the two area of cross section at the ends of the rail and the bottom face of the rail. As shown in the figure.

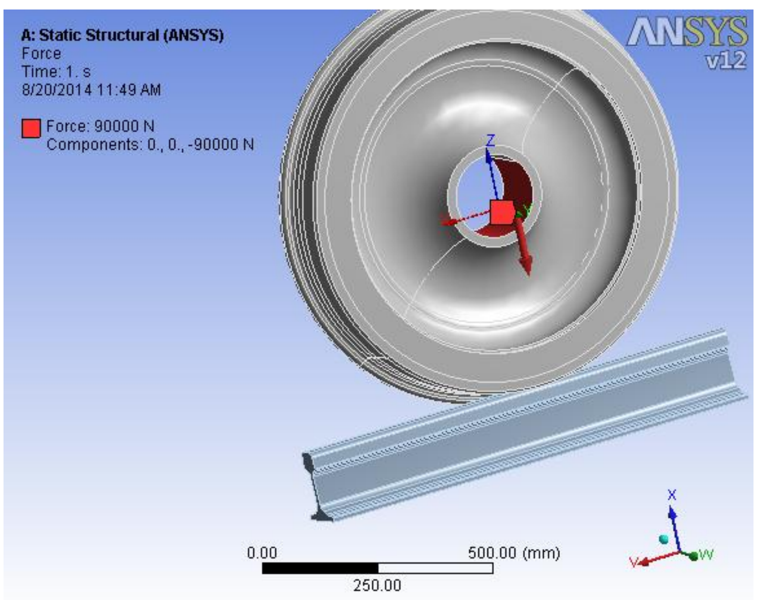

Figure 4.6: Application of vertical load for wheel rail contact assembly.

f) Wheel hub internal surfaces are selected to apply vertical load of 90KN and rotational and acceleration parameters are also employed from the specified data.

Chapter five

Results and Discussion

5.1 Effect of change of wheel taper angle (conicity) on fatigue parameters.

Table 3.4 presents the results showing effect of variation in conicity (wheel taper), designated by γ. A slight decrement in the major axis and a slight Increment in minor axis (contact width) are observed with decrease in conicity (see figure5.1). Contact area decreases with the decrease in wheel conicity resulting in an increase of the maximum contact pressure and principal stresses (see figure 5.2 and figure 5.3).

On table 3.4 it is also observed that a decrease in wheel conicity is responsible for a decrease in equivalent stress and fatigue damage and hence an increase in available fatigue life (see figure5.5). From these it is evident that a reduction in wheel taper or conicity slightly reduces expected fatigue failure.

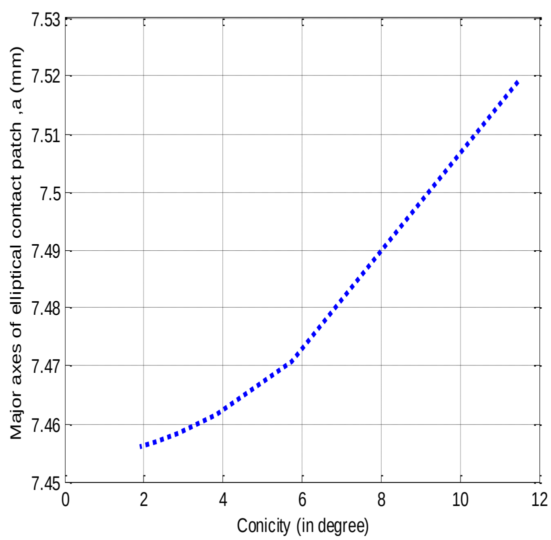

(a)

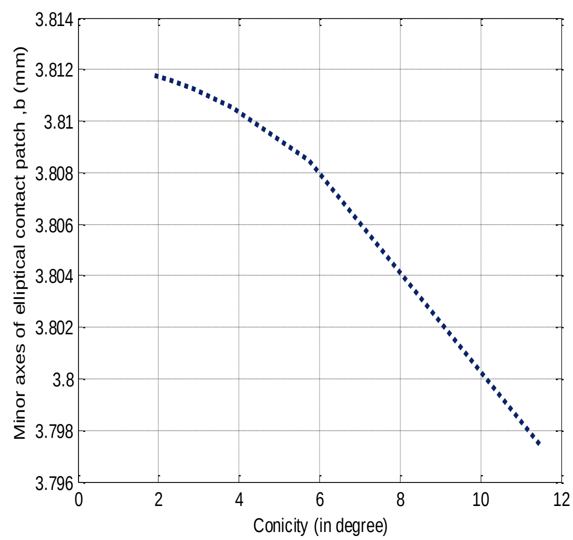

(b)

Figure5.1:(a) and (b) shows the variation of the major axes 'a' and and minor axes 'b' with the increase in wheel taper angle(conicity),γ.

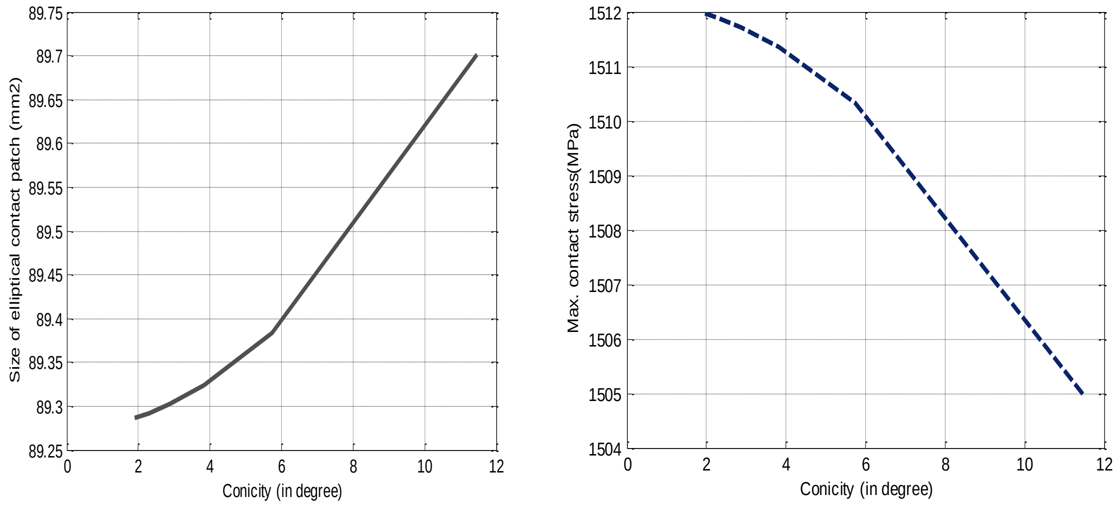

(a) (b)

Figure 5.2:(a) and (b) shows the relation ship between conicity with contact area and the maximum contact pressure respectively.

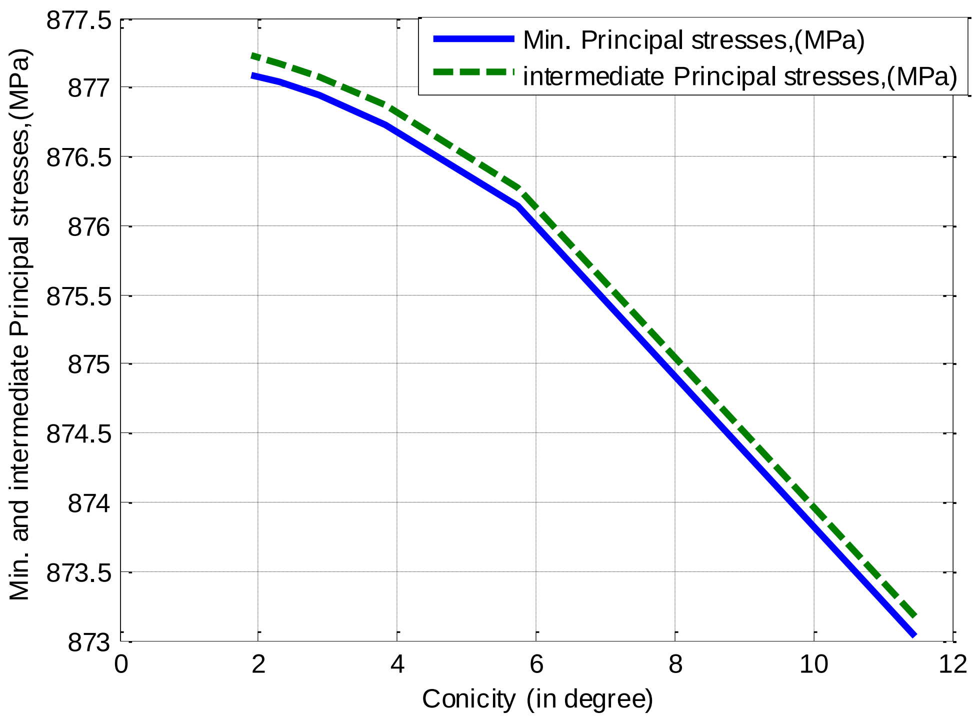

Figure 5.3: Relation ship between conicity and minimum and intermidiate principal stresses σ_2 ,σ_3

As disscussed in chapter 3, lateral and longitudinal creep forces are related to friction which are responsible for wheel wear. From equation (3.46) both lateral and longitudinal creep forces are directly proportional to wheel wear. Therefore to avoid wheel wear it is important to reduce creep forces.

In table (3.4) The decrease in conicity of wheel profile leads to slight improvement in available stress fatigue life. It is also observed in figure (5.4) that the magnitude of the the lateral and longitudinal creep forces decrease with a decrease of conicity . From these, it is evident that the use of small conicity say 1 in 30 or 1 in 40 can be established so as to decrease both rolling contact fatigue and wheel wear.

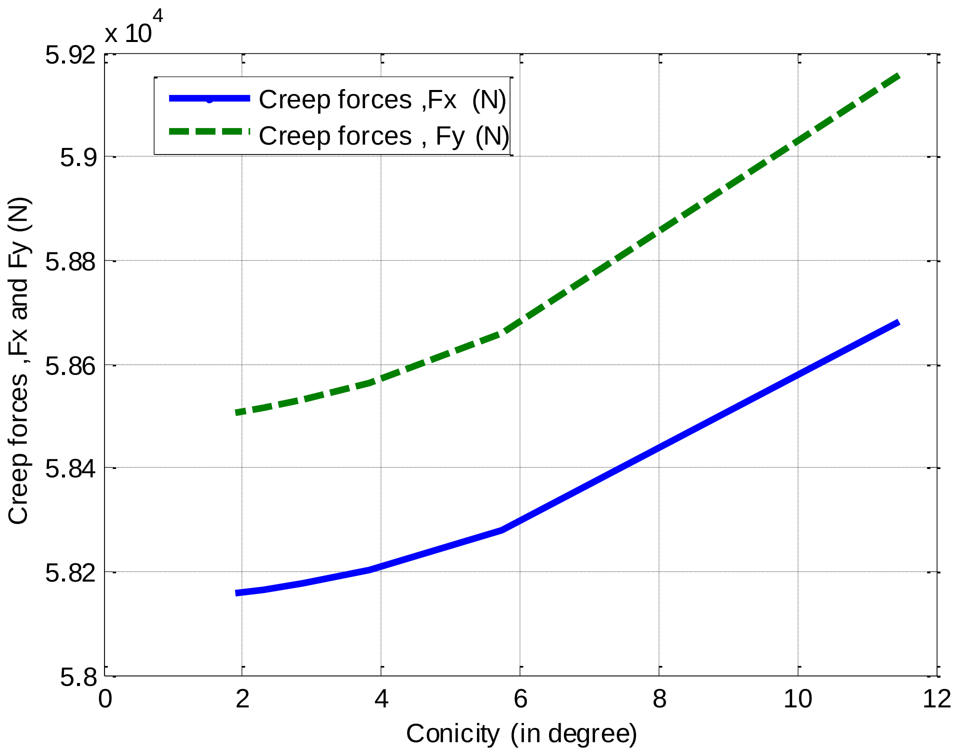

Figure 5.4:Shows the increment of longtudinal and lateral creep forces with increase of wheel taper angle (conicity)

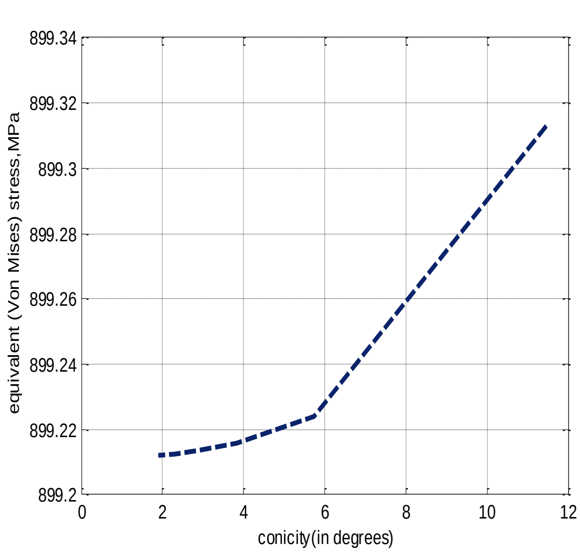

(a)

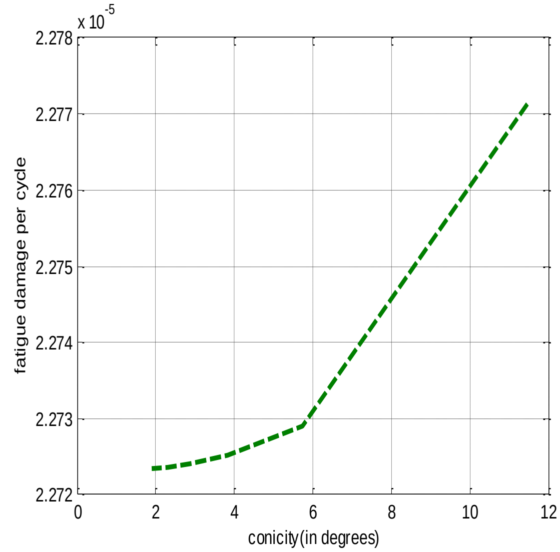

(b)

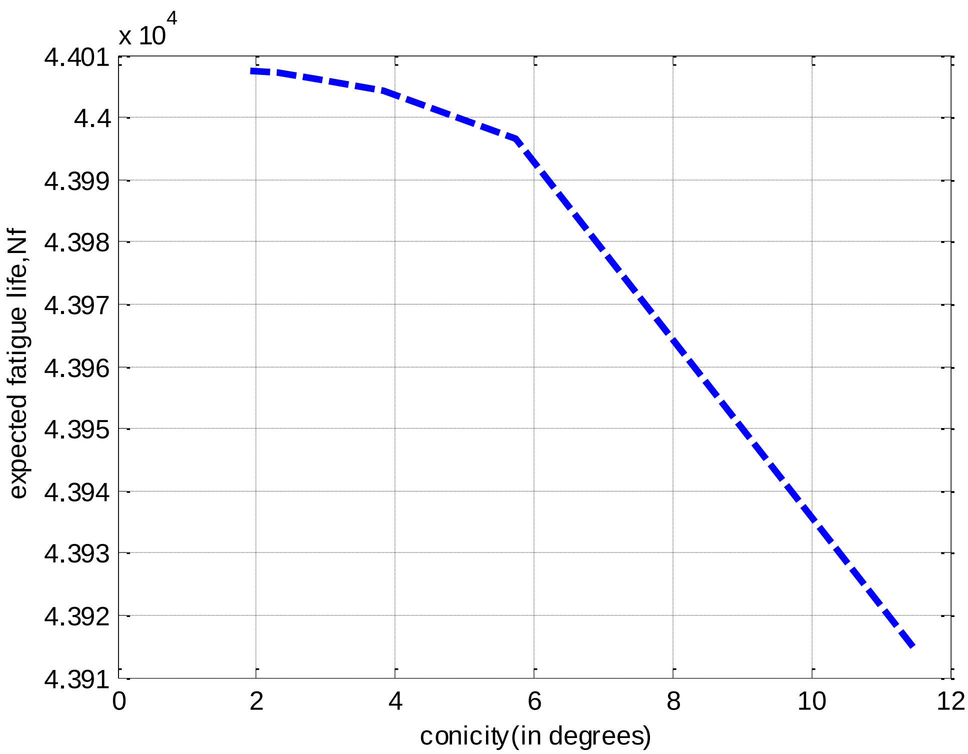

(c)

Figure 5.5:Shows how fatigue parameters vary with variation in wheel taper.(a) and (b) show how equivalent stress and fatigue damage per cycle increase with an increase in conicity respectively whereas (c) indicates the increment of expected fatigue life with a reduction in wheel conicity.

5.2 Effect of change of radius of curvature of wheel on fatigue parameters.

Effect of variation in the radius of curvature of wheel profile on contact parameters is shown in Table (3.5). Increase in contact width and reduction in contact length is observed with the increase of radius of curvature of wheel (see figure 5.6). Size of area of contact patch has increased with the increase in radius of curvature of the wheel (see figure 5.7 also see table 3.5). Contact pressure and principal stresses shows reduction with increase in wheel profile radii (figure 5.7).

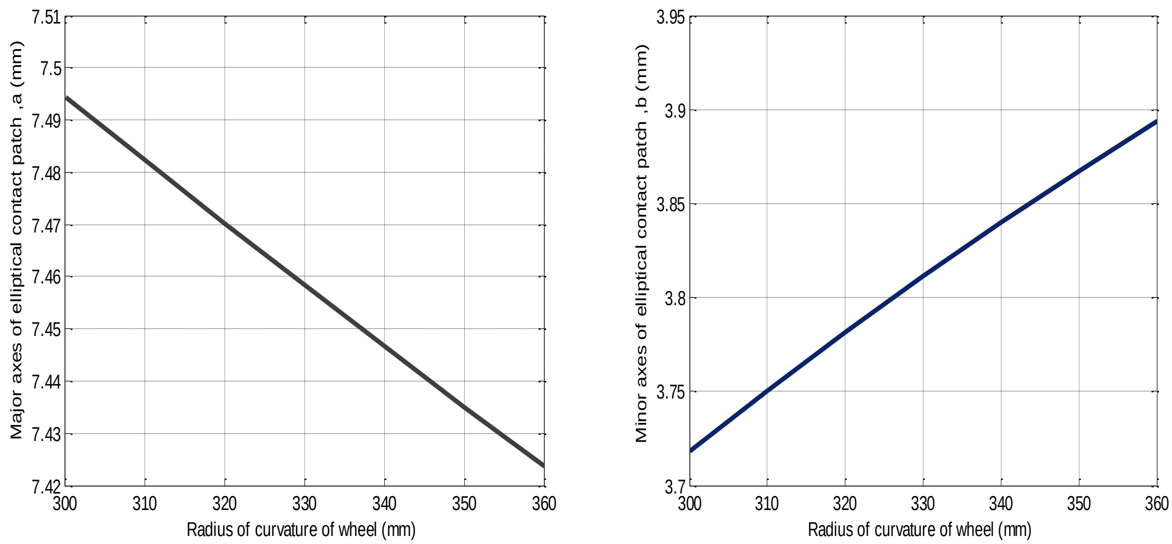

(a) (b)

Figure 5.6.(a) and (b)Shows the variation of the major axes 'a' and minor axes 'b' with the increase in radius of curvature of wheel profile.

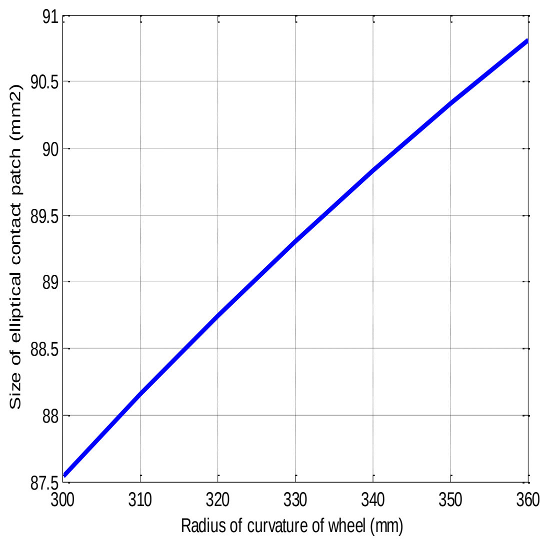

(a)

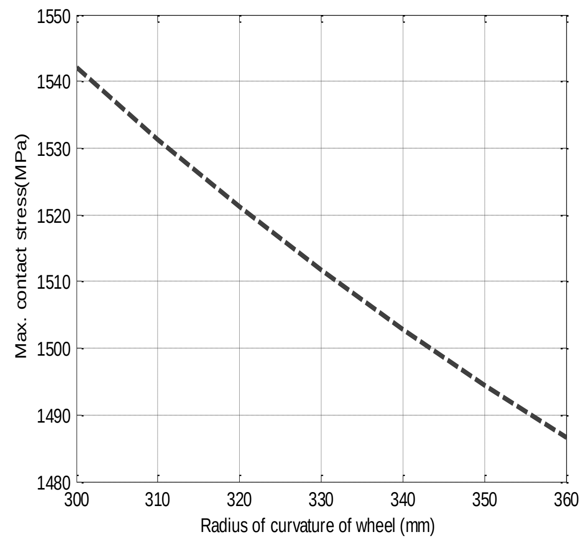

(b)

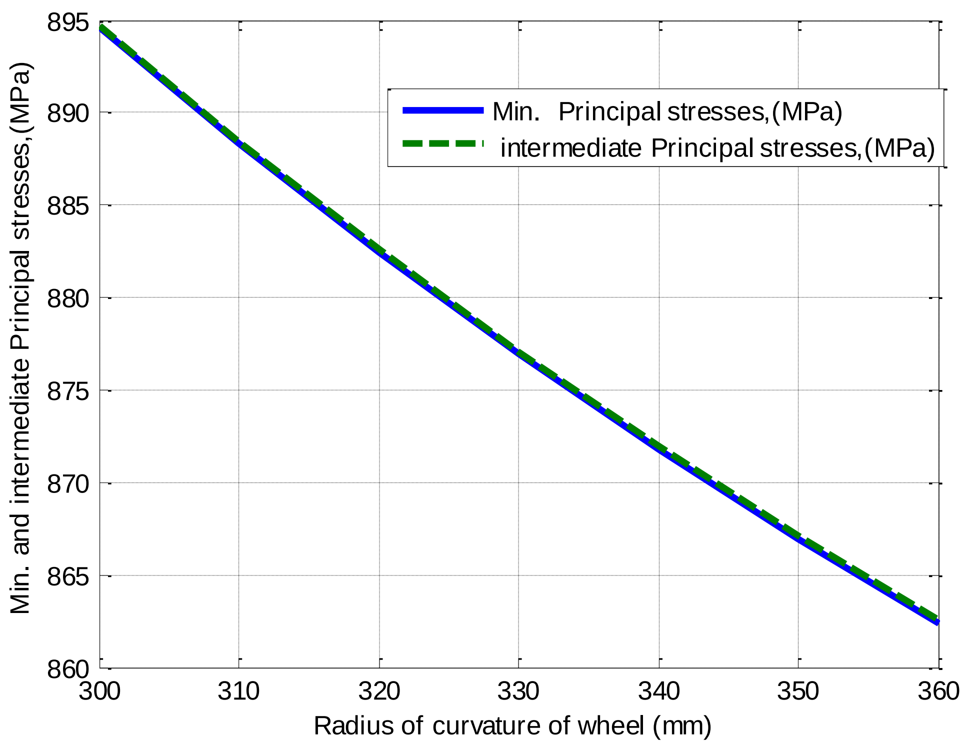

(c)

Figure 5.7: (a), (b) and (c) shows the relation ship between radius of curvature of wheel with contact area, maximum contact pressure ,and minimum and intermidiate principal stresses respectively.

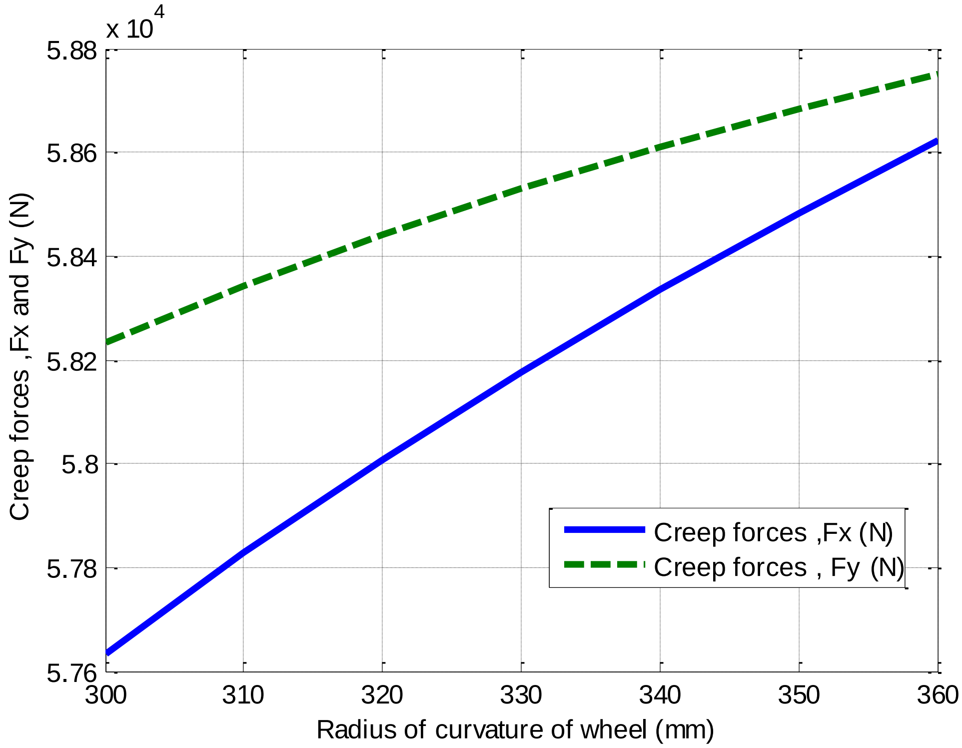

Figure 5.8: The increment of longtudinal and lateral creep forces with increase of radius of curvature of wheel profile.

Here also, the increment of lateral and longitudinal creep forces are shown with increase in the transversal radius of curvatures of the wheel (see figure5.8). As mentioned above ,these forces increases friction which is responsible for wheel wear.

Equivalent stress and fatigue damage shows reduction with an increase in radius of curvature of the wheel which leads to an increase in available wheel life. For instance, a slight increase in the radius of curvatures of wheels from 320 to 330mm results in a change in stress fatigue life from 39891 to 44006.which is a difference of 4115 available stress fatigue life cycles. (see figure 5.9 also table 3.5). The increase in radius of curvature of wheel profile leads to reduction of fatigue damage.on the other hand ,it generates high friction which leads to material wear.

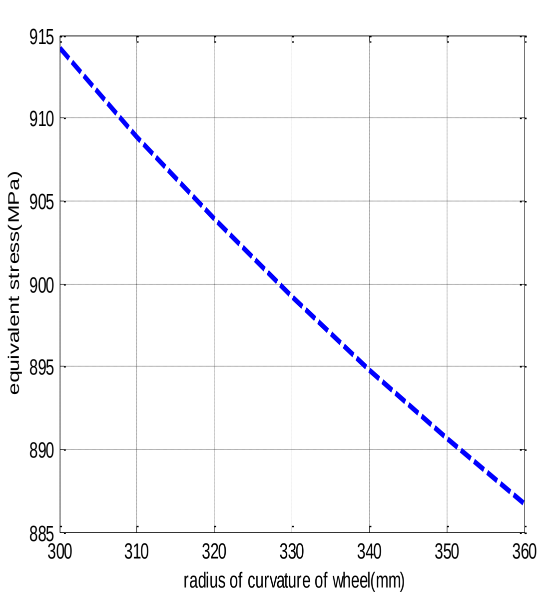

(b)

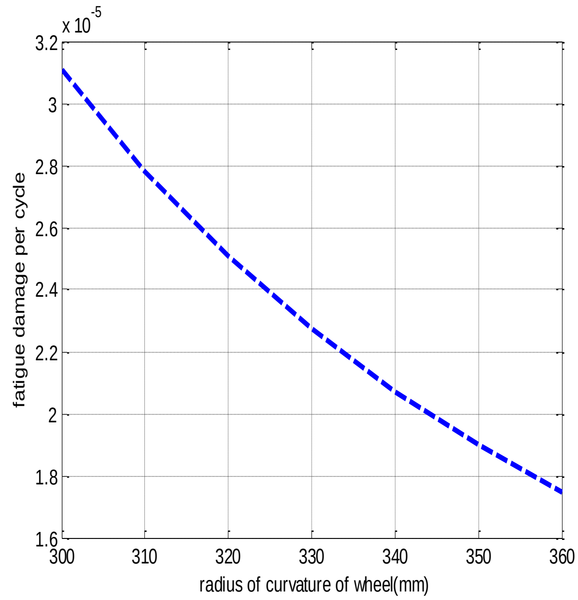

(c)

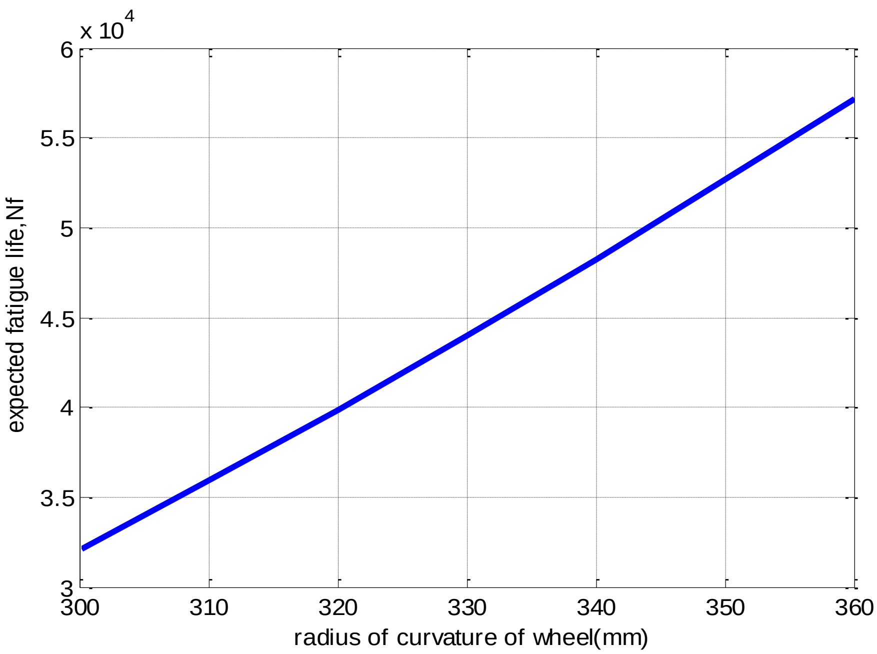

Figure 5.9: Shows the relation ship between radius of curvature and fatigue parameters.(a) and (b) shows reduction of equivalent stress and fatigue damage per cycle versus radius of curvature of wheel profile respectively.(c) shows the increment of expected fatigue life with an increase of radius of curvature of wheel profile.

5.3 Effect of change of radius of curvature of rail on fatigue parameters

Effect of variation in the radius of curvature of rail profile on contact parameters is shown in Table 3.6. Similar to the effect of change of wheel profile discussed in section 5.2, increase in contact width and reduction in contact length is observed with the increase of radius of curvature of the rail profile (see figure5.10). Size of area of contact patch has increased with the increase in radius of curvature of the wheel (see figure5.11 (a)). Contact pressure and contact stress shows reduction with increase in wheel profile radii (figure5.11 (b), (c), (d)). Similar trend is observed with varying the radii of curvatures of wheel profile, tabulated in Table3.5. As the results summarized in table 3.6 indicate the difference of contact areas are very small but the consequence is significantely very large fatigue damage.

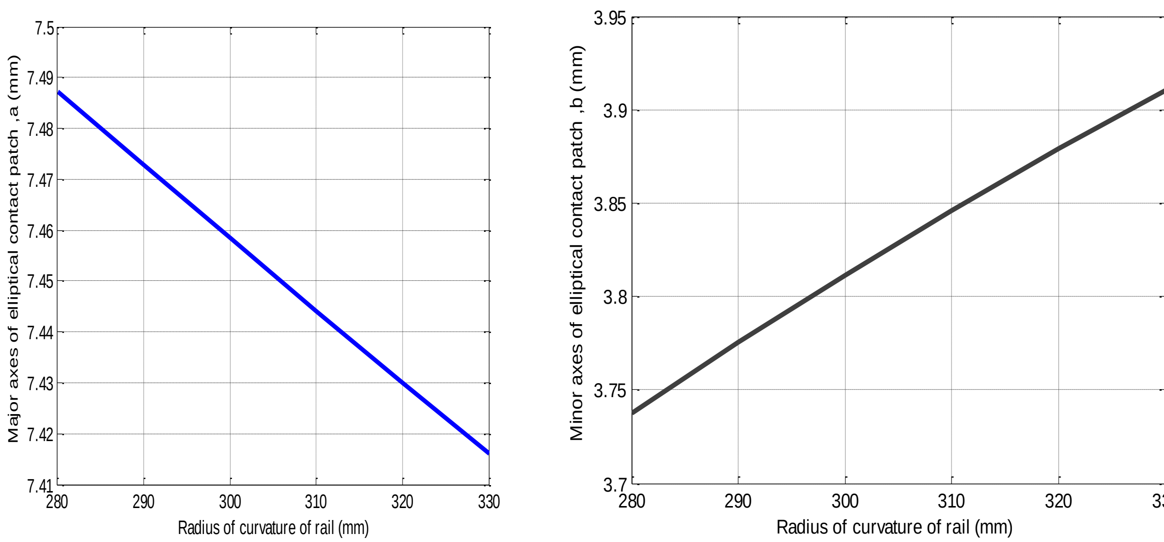

(a) (b)

Figure 5.10:(a) and (b) Shows the variation of the major axes 'a' and minor axes 'b' with the increase in radius of curvature of rail profile.

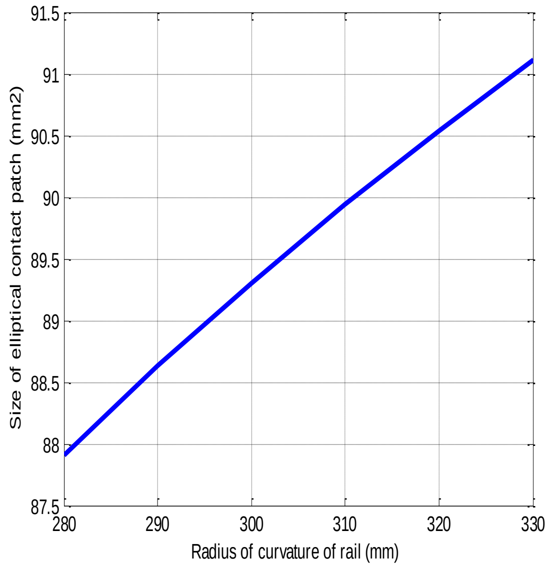

(a)

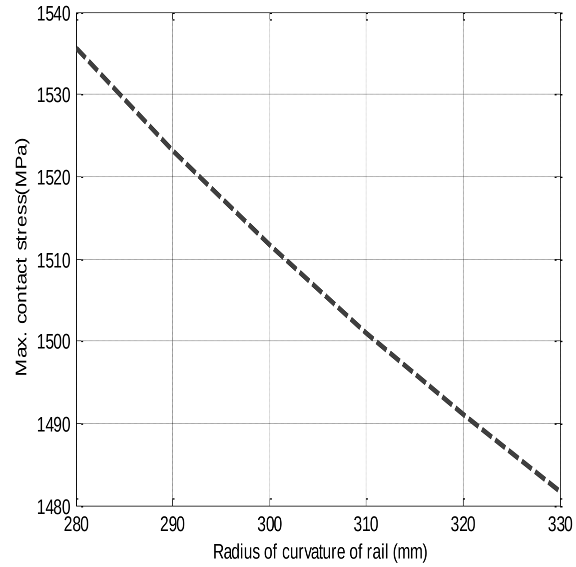

(b)

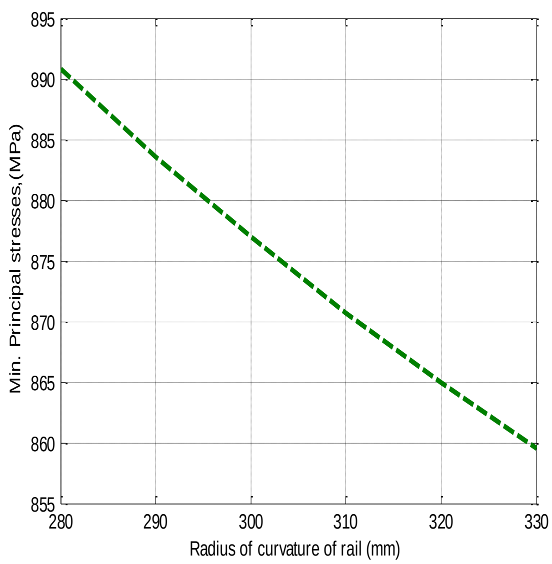

(c)

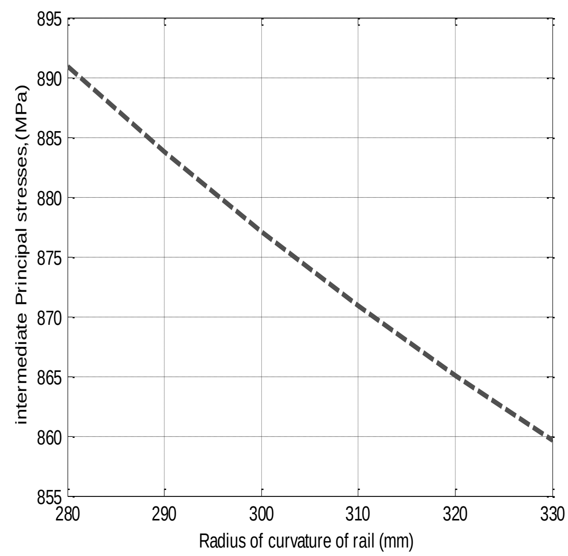

(d)

Figure 5.11:(a), b, (c) ,and (d) shows the relation ship between radius of curvature of rail with contact area, maximum contact pressure,minimum principal stress,and intermidiate principal stress respectively.

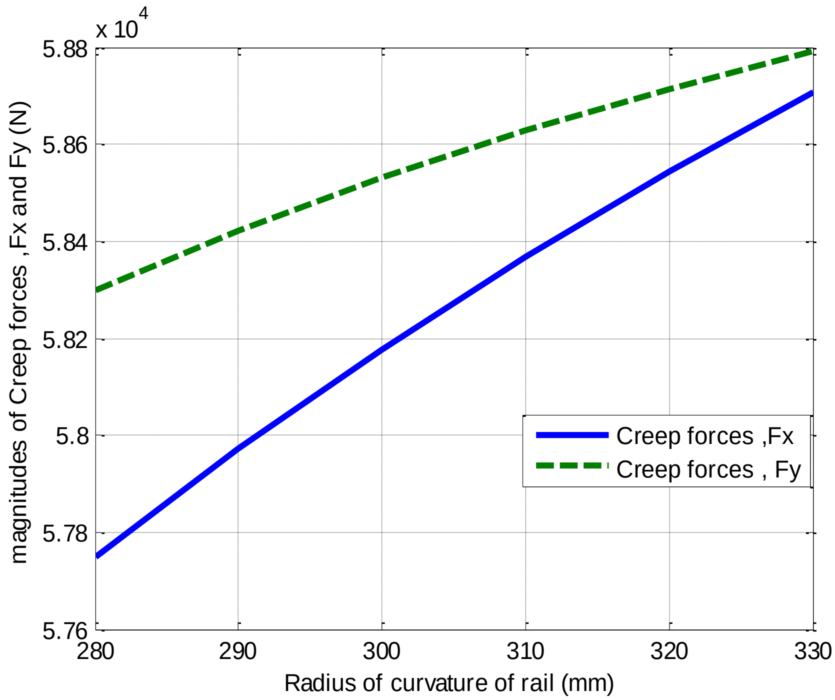

Figure 5.12: The increment of longtudinal and lateral creep forces with increase of radius of curvature of rail profile.

similar increments of results of the magnitudes of creep forces are observed as that of wheel when the radius of curvatures of rail increases. Similar to wheel studied in section 5.2, The increase in radius of curvature of wheel profile leads to reduction of fatigue damage.on the other hand ,it generates high friction which leads to wheel and rail wear.(see figure 5.12)

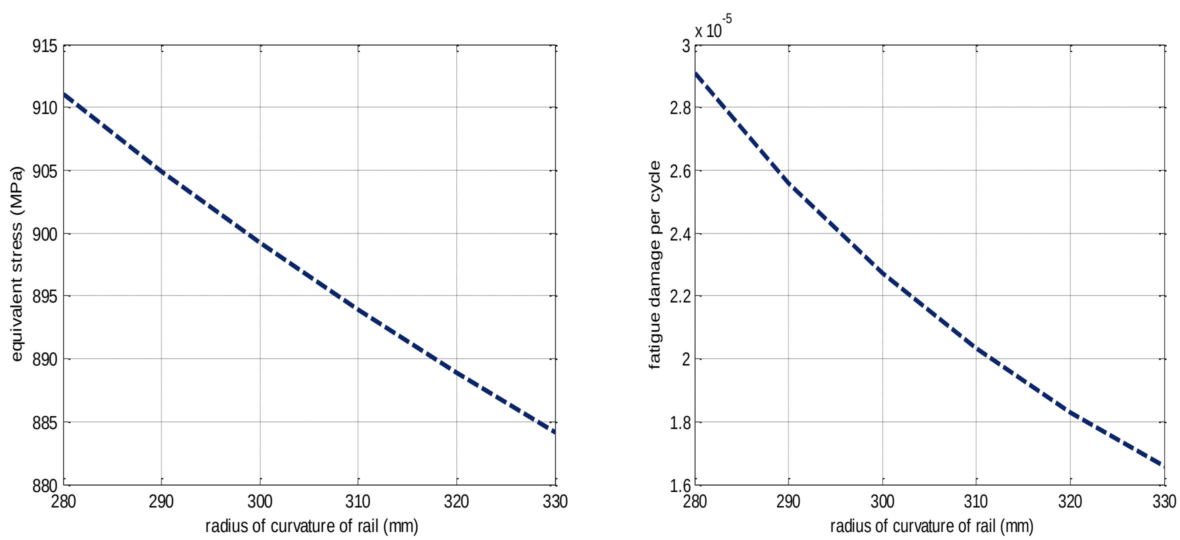

(a) (b)

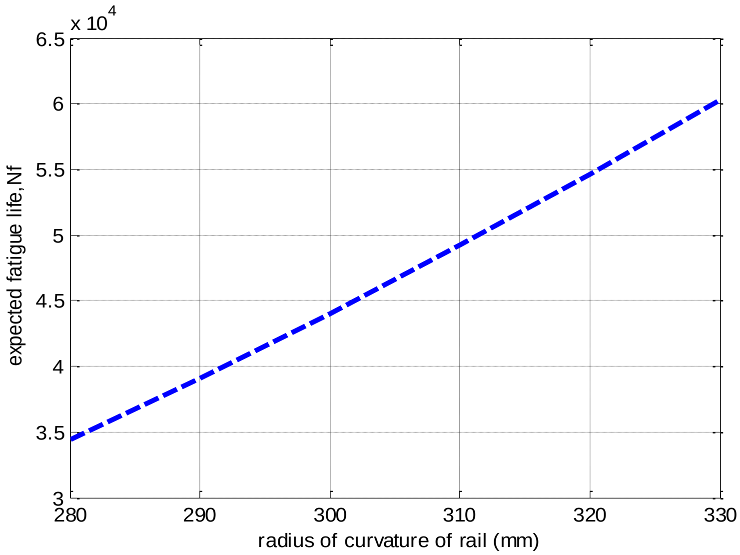

(c)

Figure 5.13: The relation ship between radius of curvature of rail and fatigue parameters.(a) and (b) shows reduction of equivalent stress and fatigue damage per cycle versus radius of curvature of rail profile respectively.(c) shows the increment of expected fatigue life with an increase of radius of curvature of rail profile.

5.4 ANSYS results

Here the finite element (approximate) results computed by ANSYS workbench are presented. Six models for different radius of curvatures of the rail at the contact region ranging from 280 to 330mm are investigated. A standard rail as per Chinese national railways standard (GB 50kg) profile for the rail and UIC-812-3-84 standard wheel is chosen for the task as illustrated in chapter4.

Figure (5.14) shows contour plot of the Von Mises stress distribution for the variation in the radius of curvatures of the rail around the critical contact point.

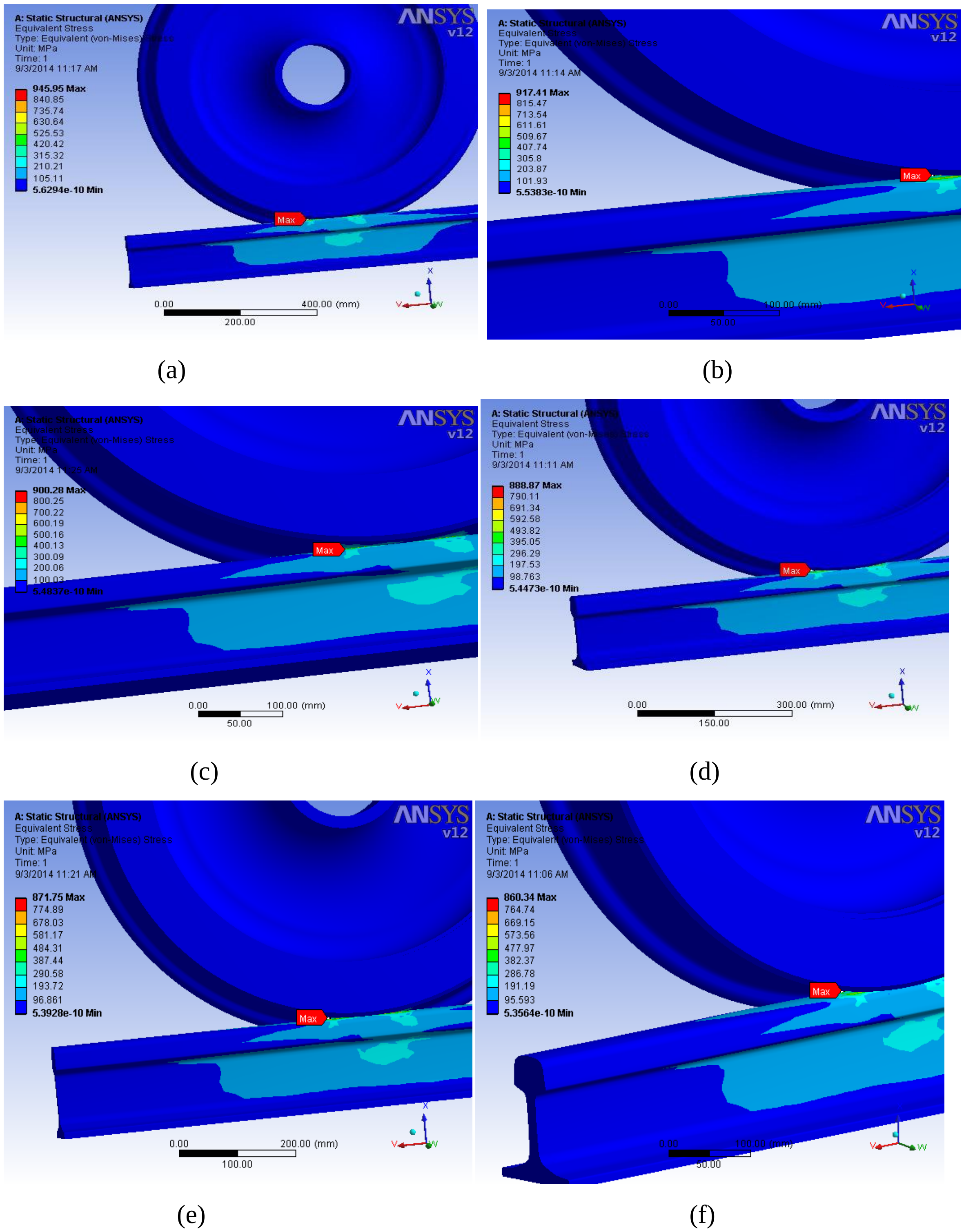

(a) (b) (c) (d) (e) (f)

Figure 5.14 Von Mises stress distribution when the radius of curvature of the rail in the contact region becomes 280,290,300,310,320,330mm for (a),(b),(c),(d),(e),(f) respectively.

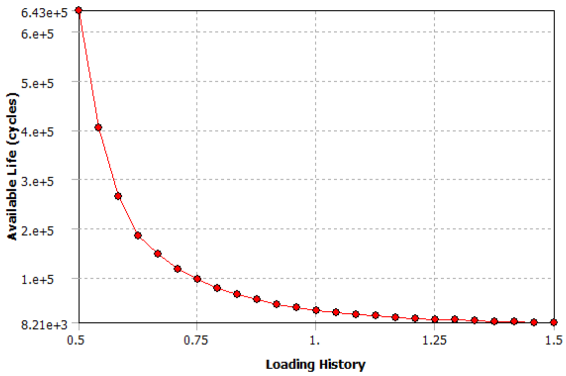

(a)

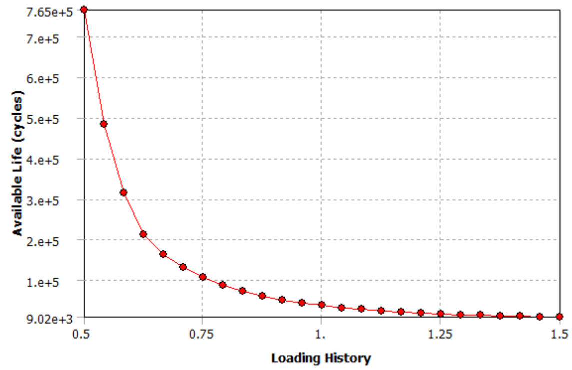

(b)

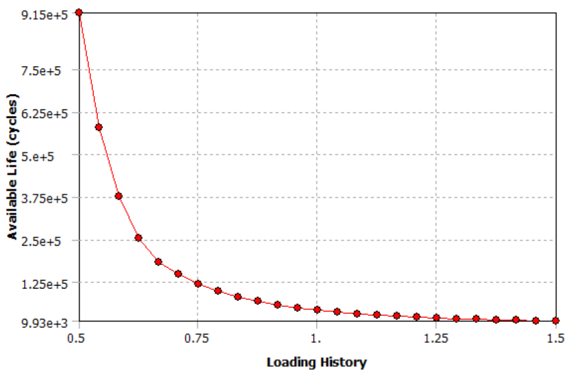

(c)

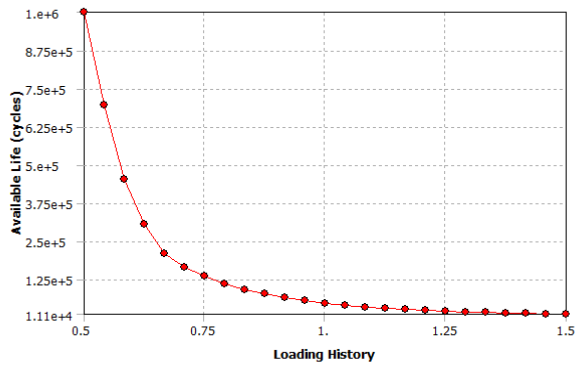

(d)

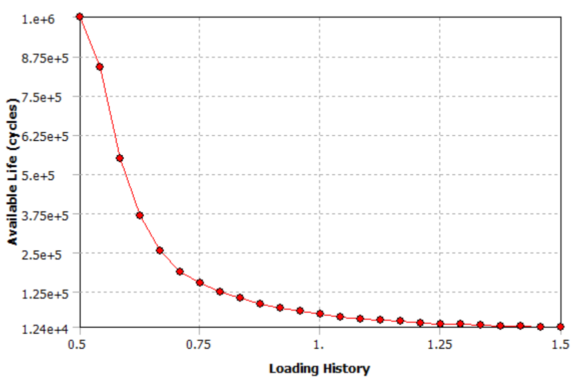

(e)

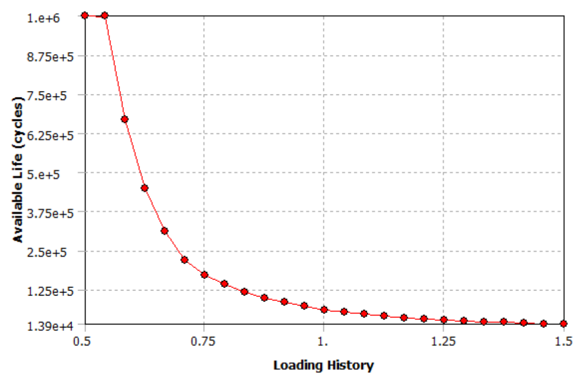

(f)

Figure 5.15: Fatigue sensitivity (available life cycles versus loading history): (a) for radius of curvature of rail=280mm (b) for radius of curvature of rail=290mm, (c) for radius of curvature of rail=300mm, (d) for radius of curvature of rail=310mm, (e) for radius of curvature of rail=320mm, (f) for radius of curvature of rail=330mm

The plots of fatigue sensitivity shows how the fatigue life changes as a function of the loading history around the critical point for the six different contact situations .the results on figure (5.15) shows the ANSYS result of the fatigue life for non constant loading and is directly obtained from ANSYS workbench analysis results .

On the other hand, the contour plot represents the number of cycles around the critical contact point until the part will fail due to fatigue. Figure (5.16) shows contour plot of the fatigue life for the variation in the radius of curvatures of the rail around the critical contact point. From the FEA requirement in a constant amplitude analysis, if the alternating stress is lower than the lowest alternating stress defined in the S-N curve, the life at that point is acceptable.

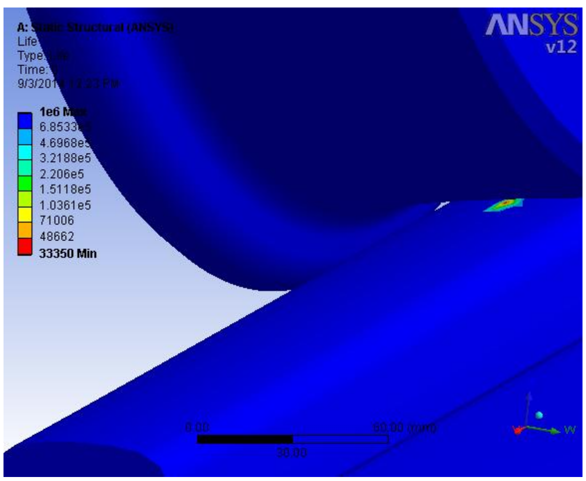

(a)

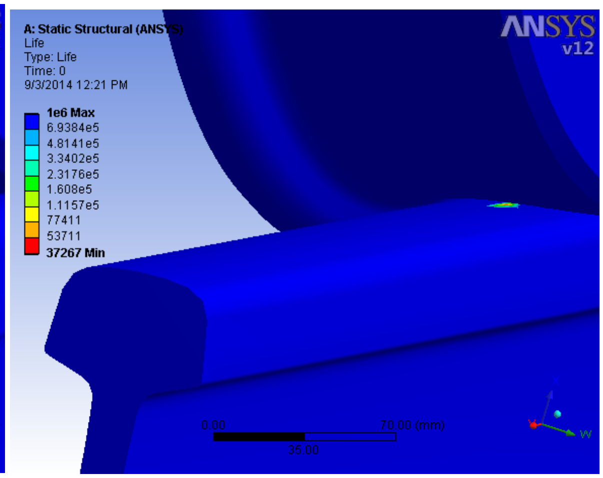

(b)

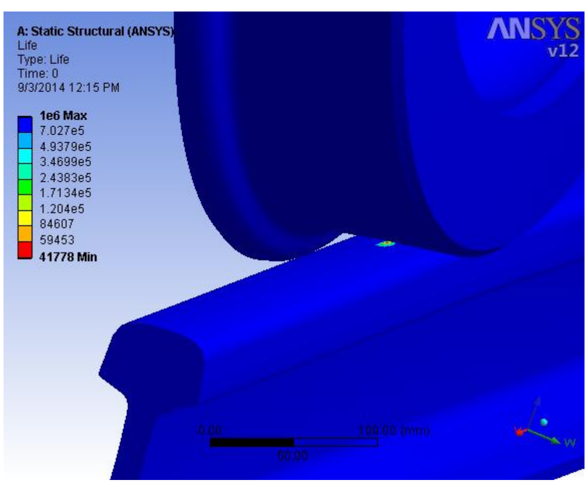

(c)

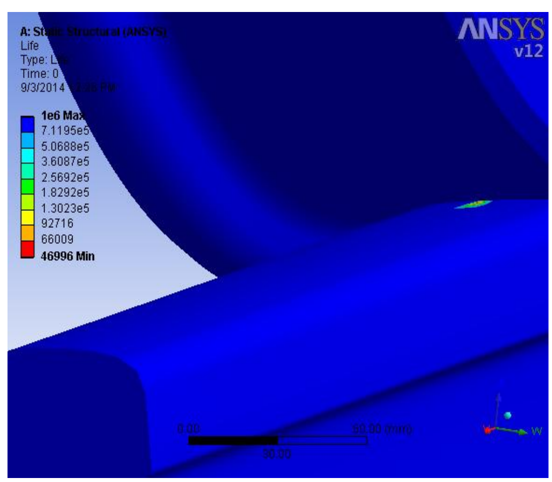

(d)

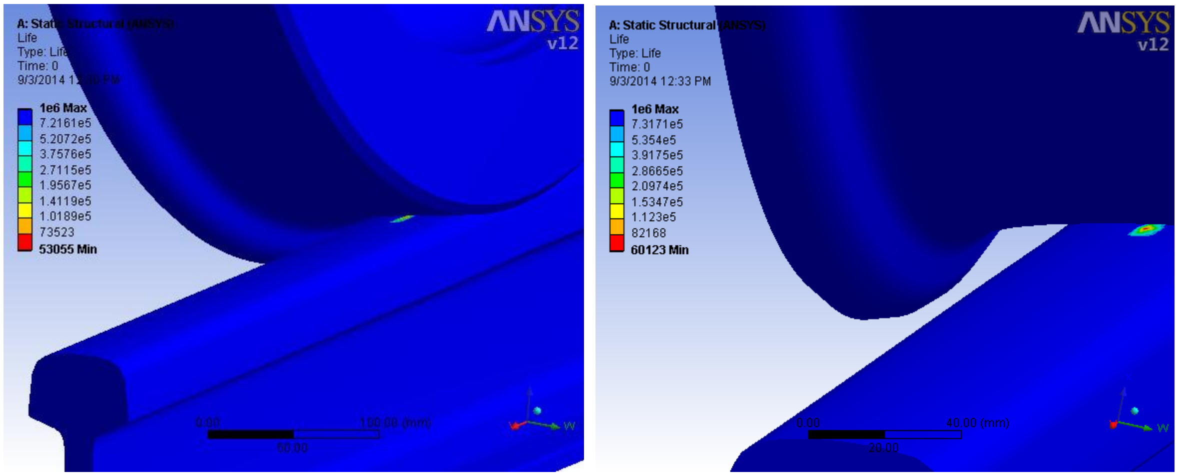

(e) (f)

Figure 5.16: Number of available fatigue life cycles (a) for radius of curvature of rail=280mm (b) for radius of curvature of rail=290mm, (c) for radius of curvature of rail=300mm, (d) for radius of curvature of rail=310mm, (e) for radius of curvature of rail=320mm, (f) for radius of curvature of rail=330mm

Table 5.1: Comparison of the theoretical and finite element results of expected stress fatigue life.

Transversal radius of curvature of rail profile (mm) at the contact point	Theoretical(analytical) results of the available fatigue life	ANSYS workbench results of the available fatigue life	Error in percent, (%)
280	34379	33350	2.9931
290	39054	37267	4.5757
300	43996	41778	5.0414
310	49191	46996	4.4622
320	54622	53055	2.8688
330	60276	60123	0.2538

Table 5.2: Comparison of the theoretical and finite element results of Von Mises (equivalent) stress for variable radius of curvatures of rail profiles.

Transversal radius of curvature of rail profile (mm) at the contact point	Theoretical (analytical) results of the Von Mises (equivalent) stress.(MPa)	ANSYS workbench results of the Von Mises (equivalent stress.(MPa)	Error in percent, (%)
280	911.0084	945.9500	-3.8355
290	904.9171	917.4100	-0.7027
300	893.8928	900.2800	-0.7145
310	893.8928	888.8700	0.5619
320	888.8892	871.7500	1.9282
330	884.1845	860.3400	2.6968

Therefore, as shown in table (5.1) and table (5.2) the ANSYS workbench indicates comparable results as that of the theoretical one.

Chapter 6

Conclusion Recommendation and future works

6.1. Conclusion

On results and discussion section, fatigue parameters variation with a slight variation in geometry of wheel and rail profiles is shown. In table 3.4 the decrease in conicity of wheel profile leads to slight improvement in available stress fatigue life.It is also observed in figure 4.8 that the magnitude of the the lateral and longitudinal creep forces decrease with a decrease of conicity .From these it is evident that the use of small conicity decreases both rolling contact fatigue phenomenon and wheel wear.

On the other hand, higher radius of curvature for wheel and rail profiles promotes a reduction on rolling contact fatigue.For instance, if Japanize industrial standard JIS 37kg and British Standard BS70Ibs A rails with radius of curvature R=304.80mm are compared to chineese national railway standard GB 50kg rail , with radius of curvature R=300mm ,which is operational for Addis Ababa Light Rail Train, a slight increment of radius of curvature of 4.80mm can be deduced from the rail profiles at the contact region .Under the same vehicle specification ,this slight variation of radius of curvature generates an increase in contact area of magnitude 0.30576mm^2 which is responsible for a reduction in the maximum contact pressure of 5.14MPa and consequentely an increase in expected fatigue life of 2493.6 cycles and these can be calculated from table 3.6. Other standard rail profiles such as Japanise industrial Standard JIS 60kg (radius of curvature 600mm) and Russian Standard GOST P 65kg(radius of curvature 500mm) has an enormous reduction in wheel fatigue damage compared to chinese GB 50kg standard rails and posseses significantely better wheel fatigue life. However, higher radius of curvature for wheel and rail profiles generates increased lateral and longtudinal creep forces which are related to friction which in turn is directely related to wheel wear as disscussed in table 3.6.Separate studies should be taken place for wheel wear and vehicle stability for optimization of wheel and rail profiles.Obviously, better wheel rail performance can be achieved compromizing all these elements .The objective of these study ,however is to show how rolling contact fatigue parameters vary with different geometrical conditions of wheel and rail profile

6.2 Recommendation

As long as the target is to decrease rolling contact fatigue phenomenon the smallest conicity is recommendable. Smallest conicity also allows reduced friction as already discussed above which is responsible for wear. However there are other design requirements where friction might be necessary, for instance braking. The lateral stability of the vehicle is also another important design requirement related to wheel rail contact.

Use of increased Transversal Radius of curvatures of both wheel and rail significantly reduces contact fatigue stresses but the problem to this end is friction which is related to wheel wear. Therefore, there must be a balance in the design process of wheel and rail profiles between a reduction in rolling contact fatigue phenomenon and decreasing wheel wear when dealing with the curvatures of the profiles.

6.3 Future works

On the present study wheel rail contact is taken into consideration at the wheel tread rail head contact which is mainly a contact zone on a straight track. Hertizian contact assumptions can be applicable in these zones. However, on curves of a track contact will be shifted from wheel tread rail head to wheel flange rail guage corner. Hertizian theories cannot be applied in these zones because one of the assumptions of Hertizian theory is to take large curvature radius compared to the contact size. However, the radii of curvatures in these zones are very small and Hertizian assumption will be inaccurate. Only finite element approaches can give us a better solution. Future researchers are expected to investigate what rolling contact fatigue is like for effect of changes of geometrical configurations of wheel and rail profiles in these zones.

As seen on chapter3, the size of the contact patch *(πab)* will influence the magnitude of the fatigue impact (σ_{EQ}).In addition, the shape of the contact patch will have an influence. In wheel-rail contact, the patch is normally elongated *($a > b$)* in the rolling direction.

The predictions of rolling contact fatigue in this thesis reflect the exponential growth of the fatigue damage based on the Dang Van equivalent stress. It simply predicts general fatigue damage based on stress. It does not identify crack initiation and crack propagation.

Therefore, fatigue prediction related to the geometry of wheel and rail profiles is limited to surface crack initiation and subsurface crack initiation from some 4mm to 10mm below the wheel tread (i.e. shallow initiation). Crack propagation and deeper crack initiations (at some 10 to 25mm below the tread) has less dependency on contact geometry. Therefore, better approximations of fatigue predictions related to contact geometry is required in order to optimize wheel and rail profiles.

Reference

1. CRN RS 006: Minimum Operating Requirements For Road Rail Infrastructure Maintenance Vehicles: Version1.0 Issued December 2011,Principal Rolling Stock Engineer,USA 2011.

2.Iwnicki S. (ed.), (2006) Handbook of railway vehicle dynamics, CRC Press, Taylor & Francis Group, 2006, ISBN-13: 978-0-8493-3321-7.

3.Ivan Y. Shevtsov: Wheel/Rail Interface Optimization ,Section of Road and Railway Engineering Faculty of Civil Engineering and Geosciences, Delft University of Technology Delft, Netherlands, 2008

4. Branislav Sladojevic, Milos Jelic, Milica Puzic: New Requirements for The Quality Of Steel Rails, 4th International Conference Processing and Structure Of Materials Held On Palic, Serbia May 27- 29, 2010

5. Tanel Telliskivi: Wheel-Rail Interaction Analysis, Department of Machine Design Royal Institute of Technology, Kth Se – 100 44 Stockholm, Sweden, 2003

6. Gunter Schupp , Christoph Weidemann And Lutz Mauer, 2007,Modeling The Contact Between Wheel And Rail Within Multibody System Simulation German Aerospace Center, Institute Of Aero Elasticity, Germany

7. Ulf Olofsson and Roger Lewis: Hand book of rail way vehicle dynamics, Tribology of the Wheel – Rail Contact ,Taylor & Francis Group, LLC , pp.121-138,2006

8. Eric Magel, Peter Sroba, Kevin Sawley and Joe Kalousek : Control of Rolling Contact Fatigue of Rails ,Centre for Surface Transportation Technology, National Research Council ,Canada ,2006

9 Pislaru, Crinela (2012) :Modelling and Simulation of the Dynamic Behaviour of Wheel-Rail Interface, In: IET Event: The Railway Wheel-Rail Interface: Damage Mechanisms and Potential Solutions, 5 March 2012, University of Huddersfield .

10. Gunter Schupp , Christoph Weidemann And Lutz Mauer, 2007,Modeling The Contact Between Wheel And Rail Within Multibody System Simulation German Aerospace Center, Institute Of Aero Elasticity, Germany

11. Paul Boyd, Manicka Dhanasekar: Wheel / Rail Contact Analysis
Central Queensland University, Centre for Railway Engineering, Qld 4702, Australia, 2002

12 Marine Vidaud, Dr. Willem-Jan Zwanenburg : Current situation on rolling contact fatigue – a rail wear phenomenon, Swiss Transport Research Conference , Monte Verita /Ascona ,*Sept 9 - 11*, *2009*

13. F. Carter, On the action of a locomotive driving wheel, Proc. R. Soc. London 112 (1926) 151–157.

14. K. Johnson, Contact Mechanics, Cambridge University Press, Cambridge, 1985.

15. J. Kalker, Three-Dimensional Elastic Bodies in Rolling Contact, Kluwer Academis Publishers, Dordrecht, 1990.

16 P. Wriggers, Computational contact mechanics, John Wiley & Sons
Ltd., Chichester, 2002.

17. Matin Shahzamanian Sichani: Wheel-Rail Contact Modelling in Vehicle Dynamics Simulation, KTH Engineering Sciences, Licentiate Thesis Stockholm, Sweden 2013

18.Kapoor, A (1994), Re-evaluation of the life to rupture of ductile metals by cyclic plastic strain, Fatigue & Fracture of Engineering Materials & Structures, 17(2), 201-19.

19.Kabo, E., Ekberg, A., 2005. Material defects in rolling contact fatigue of railway wheels – the influence of defect size. Wear 258 (7–8), 1194–1200.

20.Kabo, E., 2002. Material defects in rolling contact fatigue of railway wheels – influence of overloads and defect clusters.International Journal of Fatigue 24 (8), 887–894.

21.Hrennikoff, Alexander (1941). "Solution of problems of elasticity by the framework method".

22.Kabo, E., 2002. Material defects in rolling contact fatigue of railway wheels – influence of overloads and defect clusters.International Journal of Fatigue 24 (8), 887–894.*Journal of applied mechanics* **8.4**: 169–175.)

23.Kabo, E., Ekberg, A., 2005. Material defects in rolling contact fatigue of railway wheels – the influence of defect size. Wear 258 (7–8), 1194–1200.

24.Michael G/mariam, Effect of Change of Contact Ratio on Contact Fatigue Stress of Spur Gears: Addis Ababa University School Of Graduate Studies, Addis Ababa, 2013